THE APPLICATION OF PRACTICAL PRESSURE-TRANSIENT MODELS TO INTERPRET MULTI-FRACTURED HORIZONTAL WELLS IN UNCONVENTIONAL SHALE RESERVOIRS

A Thesis

by

FABIAN ANTHONY JIMENEZ

Submitted to the Graduate and Professional School of
Texas A&M University
in partial fulfillment of the requirements for the degree of

MASTER OF SCIENCE

Chair of Committee,	Thomas Blasingame
Committee Members,	Maria Barrufet
	Eduardo Gildin
	Mukul Bhatia
Head of Department,	Jeff Spath

August 2022

Major Subject: Petroleum Engineering

ABSTRACT

Modern development of hydrocarbon-bearing reservoirs in the United States is largely focused in heterogeneous, ultra-low permeability rock. In developing these reservoirs, horizontal wells with multiple hydraulic fractures are preferred. Resulting complex flow behaviors due to field development design can make field data interpretations and productivity assessments challenging. Pressure-transient analysis (PTA) can provide insightful information related to reservoir flow behavior and hydraulic fracture efficiency.

In this work, approaches are presented to evaluate field development strategies using a practical pressure-transient model and auxiliary plotting functions. Using a trilinear flow model, we show how different regions within a reservoir contribute to pressure depletion, and thus, productivity. We illustrate the flow regimes that can be expected when natural fractures are present in a reservoir. We incorporate a power-law derivative formulation to evaluate pressure diagnostics during different periods of linear flow. We evaluate how production interference events can be detected through the use of pressure derivative plotting functions.

Ultimately, the purpose of this work is to outline practical applications that pressure-transient analysis (PTA) methods can provide in the development of unconventional shale reservoirs.

DEDICATION

This thesis is dedicated to:

My grandparents, David and Berta, for planting the seeds for my success;

My parents, Fabian and Leslie, for cultivating a supportive environment for my post-graduate studies;

My sister, Briana, for inspiring me to grow as both a person and engineer.

ACKNOWLEDGEMENTS

I would like to thank my committee chair, Dr. Thomas A. Blasingame, for his support and encouragement throughout the preparation of this work. His unique approach to learning and investigating new subjects has disciplined me into a stronger and more capable engineer.

I would like to express my sincere appreciation to each of my committee members, Dr. Maria Barrufet, Dr. Eduardo Gildin, and Dr. Mukul Bhatia for dedicating their time and efforts to serve as mentors throughout my graduate studies.

Finally, thank you to all the wonderful friends and colleagues I have had the pleasure of meeting throughout my time at Texas A&M University.

CONTRIBUTORS AND FUNDING SOURCES

Contributors

This work was supervised by a thesis committee consisting of Professors Thomas A. Blasingame (chair), Maria Barrufet, and Eduardo Gildin of the Department of Petroleum Engineering and Professor Mukul Bhatia of the Department of Geology.

The development and comprehension of analytical methods presented as pressure-transient models was aided by working conversations with Dr. David Craig and Dr. Valdes-Perez, in conjunction with thesis committee members.

The data analyzed using analytical models in this work was provided by various members of the Crisman Institute for Petroleum Research (CIPR) at Texas A&M University.

All other work conducted for the thesis was completed by the student independently under the advisement of Dr. Thomas A. Blasingame of the Department of Petroleum Engineering.

Funding Sources

Graduate study was supported and made possible by the Crisman Institute for Petroleum Research (CIPR) at Texas A&M University.

TABLE OF CONTENTS

Page

LIST OF FIGURES

Page

LIST OF TABLES

Page

CHAPTER I

INTRODUCTION

In this chapter, we present the general overview of this thesis. We divided this chapter into three sections. In the first section we formally develop the problem statement related to this work. In the next section, we define the objectives of this research. Finally, we provide an outline for how this work is organized.

1.1. Statement of the Problem

Unconventional shale reservoirs characteristically have permeability values on the order of 0.001 md (1000 nd) or less. As a result, these reservoirs exhibit very long periods of transient flow (often several years, for ultra-low permeability systems this could be decades). This condition of very long transient flow, somewhat counterintuitively, makes the applications of "conventional" pressure-transient analysis (*e.g.*, radial flow, boundary limits testing, etc.) irrelevant due to impractical testing time requirements to see any reservoir features beyond fracture-dominated flow.

However, due to the productivity of a well largely being confined to the stimulated reservoir volume (SRV), it is important that this region be well understood (Medeiros, Ozkan, and Kazemi [2008]). Oil and gas operators budget a significant portion of a the capital expenditure for a given well towards the completion design (including well stimulation) and as such, the resulting fracture efficiency cannot be understated.

Knowing that the productivity of a well is largely governed by its stimulated reservoir volume, operators have *strategically* opted for tighter well spacing to limit unrecovered resources between wells. Lerza, Cuervo, and Malhotra [2021] show that inappropriately narrow well spacing (often referred to as "tight" spacing) can be detrimental to the overall productivity and recovery of a given well due to pressure depletion and "fracture driven interactions" (FDIs) which are also known as "frac-hits" in field jargon. . Detection and assessment of these inter-well interaction events can help operators mitigate the negative parent-child effects on production.

1.2. Research Objectives

We define the following objectives for this work:

- Identify a practical pressure-transient model(s) that can be used to characterize the rate and pressure performance for a multi-fracture horizontal well (MFHW) case.
- Develop plotting functions to characterize power-law flow regimes — generally these are "fracture-dominated" of "fracture-transition" flow regimes.
- Develop interpretation methods related to well interference events.

1.3. Organization of the Thesis

- Chapter I — Introduction
  - Statement of the Problem
  - Research Objectives
  - Organization of the Thesis
- Chapter II — Literature Review
  - Unconventional Reservoir Systems — Overview
  - Pressure-Transient Models for Well Intercepted by Fractures
  - Pressure-Transient Plotting Functions for Diagnostics
- Chapter III — Trilinear Flow Model for Evaluating Reservoir Performance in Unconventional Shales
  - Model Foundation
  - Development of Type Curves
  - Applications to Field Data
- Chapter IV — Application of the β-Derivative as a Diagnostic Tool for Well and Fracture Interference Analysis
  - Development of the Two-Well Numerical Model
  - Hydraulic Fracture Spacing Effects on Interference
  - Well Spacing Effects on Interference
- Chapter V — Summary, Conclusions, and Recommendations
  - Summary
  - Conclusions
  - Recommendations for Future Work
- Nomenclature
- References
- Appendix A — Additional Type Curves Generated Using the Trilinear Flow Model

CHAPTER II

LITERATURE REVIEW*

2.1. Unconventional Reservoir Systems — Overview

This section provides a brief description of unconventional reservoir systems. Geologic and petrophysical characteristics of unconventional reservoir systems are outlined to illustrate the unique challenges associated with production from these resources. Current production strategies implemented by industry to deplete these resources are discussed. Finally, an overview of the current state of United States shale (and "tight" oil and gas) resource development is provided.

Unconventional Reservoir Systems — Orientation

Figure 2.1 presents a schematic of the various targeted reservoirs related to hydrocarbon production, both conventional and unconventional. Masters [1979], Holditch [2006], and Ilk [2010] describe that unconventional resources are desirable since they are often found in larger sizes. However, they are more difficult to produce as compared to conventional reservoirs. Shale oil and gas are unconventional resources in which the source rock also serves as the reservoir rock and is drilled into for production. Tight oil and gas do not require that the target hydrocarbons be situated in the shale rock still. Tight oil and gas may be commonly found in sandstones or carbonates (*e.g.*, Figure 2.1).

*The following URTeC paper, *Application of the β-Derivative to Evaluate Multi-Fractured Horizontal Well Performance in Unconventional Shale Reservoirs*, is reprinted with permission from the Unconventional Resources Technology Conference, whose permission is required for further use.

Sonnenberg and Meckel [2016] detail some of the factors that make production from unconventional reservoirs difficult:

- Low- to ultra-low matrix permeability.
- Adsorbed gas in kerogen.
- Abnormal pressure (over-pressured reservoir compartments).

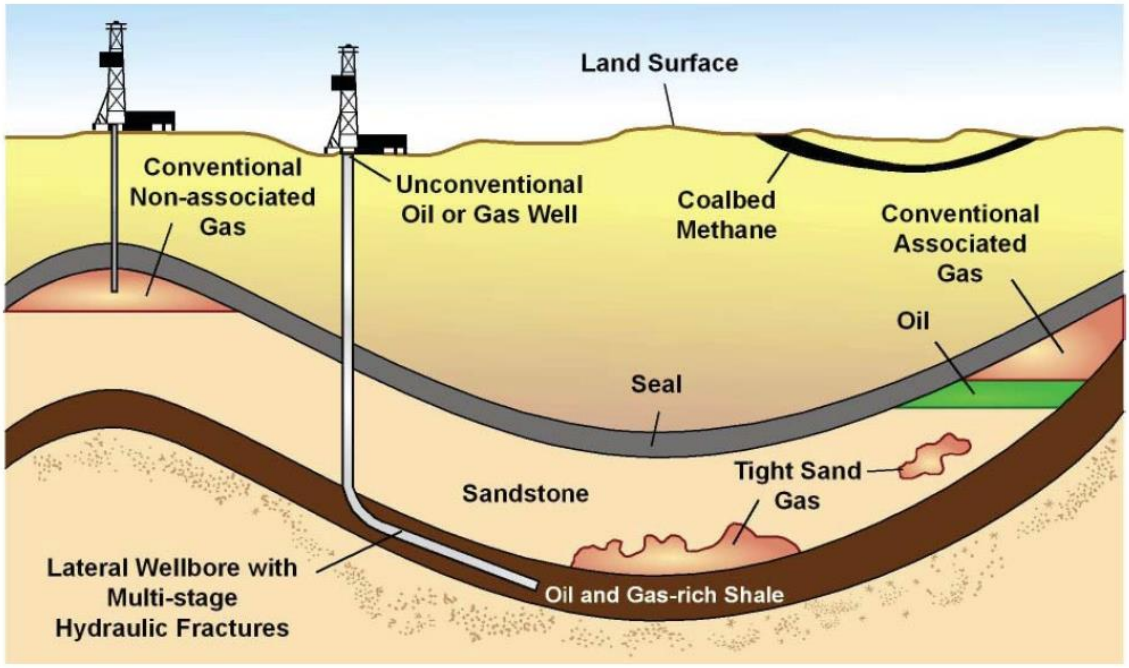

Figure 2.1 — Schematic diagram illustrating the various target reservoirs for production of hydrocarbons from both conventional and unconventional reservoirs (reprinted from US-EIA, The Geology of Natural Gas Resources, 2011).

Sondergeld *et al*. [2010] explain that unconventional reservoirs exhibit very fine grain rock texture and pore throats that are commonly micro- to nanometer in scale. In addition to this, heterogeneity effects are typically present at all scales for unconventional reservoir systems. This fact is further complicated as gas particles frequently adsorb to the surface of the fine grains and accompanying tight pore throats. Resultingly, the computation of total gas reserves (free and adsorbed) becomes complex. Experimental testing of rock samples are required in order to generate Langmuir isotherms describing the relationship between adsorbed gas content and pressure (Pathi *et al*. [2021]). These experiments may produce various results since the adsorbed gas content can vary widely based on organic matter content, pore size distribution, diagenesis, reservoir pressure and temperature (Sondergeld [2010]).

Cruz *et al.* [2020] have shown that capillary pressure forces in unconventional reservoirs are significant, and based on experimental analysis, the additional effective stress due to the capillary forces can be as large as 10,000 psi. This significant capillary pressure force leads to an effectively reduced total porosity for a given reservoir. Studies have shown that this total porosity reduction can reach values as large as 13% (Cruz *et al.* [2020]). Poe [2014] confirms the importance of capillary pressure and warns that the neglection of capillary pressure effects in low-permeability unconventional reservoirs can result in significant errors in reservoir intrinsic properties and well completion effectiveness when conducting production performance analyses.

It is clear that unconventional reservoir systems pose significant challenges for operators looking to develop them. However, with increasingly advanced technologies, optimized

production strategies, and favorable commodity pricing, these resources can be developed economically by operators.

Modern Development Strategies for Unconventional Reservoir Systems

Figure 2.2 outlines the evolution and current state (as of April 2022) of "tight oil" production in the United States. Daily oil production has experienced significant growth since 2010 with the Wolfcamp, Bakken, Spraberry, and Eagle Ford plays being responsible for the majority of this increased production. Two technologies have allowed for modern developments in these unconventional (or "tight") reservoirs to be successful: horizontal drilling and hydraulic fracturing.

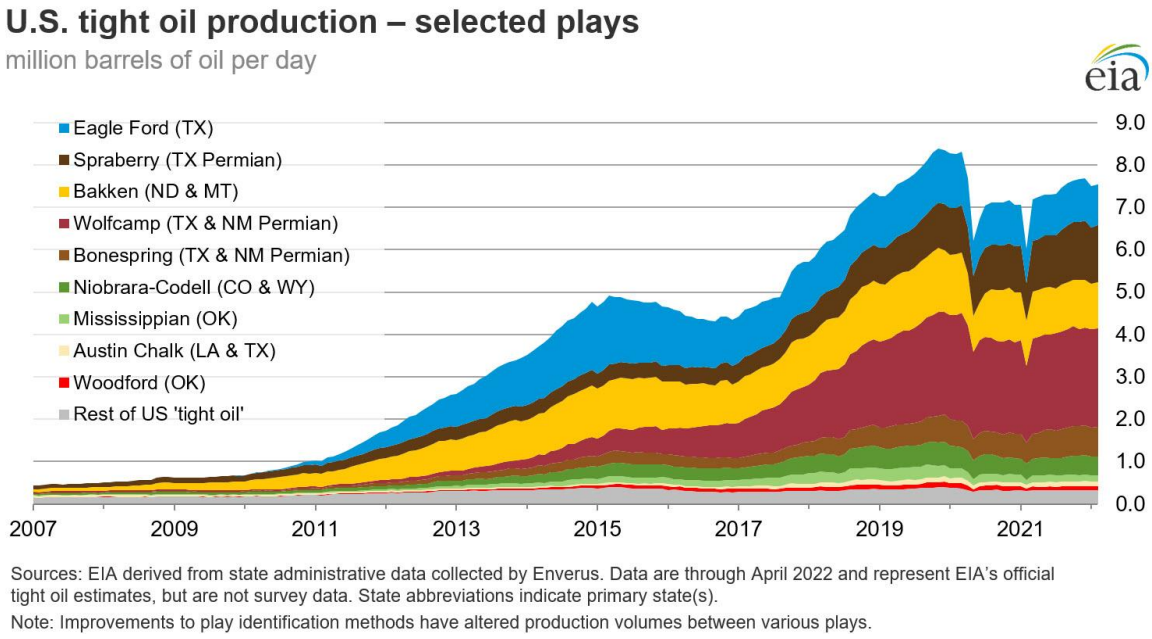

Figure 2.2 — Cartesian time-series plot for United States tight oil daily production by selected plays in million barrels. Through the development of technologies such as horizontal drilling and hydraulic fracturing, field development programs centered in "tight" formations have become favorable (reprinted from US-EIA, Petroleum & Other Liquids Data, 2022).

Horizontal Drilling

Due to the low to ultra-low matrix permeabilities unconventional reservoir systems typically possess, hydrocarbon production is largely limited to the volume contained nearby the wellbore. As a result, the development of horizontal drilling has become essential for extracting hydrocarbons from these tight oil and shale reservoirs. Beginning in 2004, horizontal wells were utilized to produce 15% of the United States crude oil from tight oil formations (US-EIA [2019]). US-EIA [2019] reports indicate that by year-end 2019 this metric has increased to 96%. Similarly, horizontal wells made up 97% of the United States natural gas production from tight formations for the same year.

As technology associated with drilling horizontal wells has evolved, operational efficiency has increased. Britt, Jones, and Miller [2010] provide an extensive study of the drilling design parameters related to developments in tight formations and their relative impact on discounted net present value. It has been shown through many examples that wellbore-to-reservoir contact is essential. From a drilling engineering perspective, the logical conclusion is to increase lateral length thus enhancing the contact surface area for production. Britt, Jones, and Miller [2010] show that the modification of this drilling design parameter yields increased annualized rates and instantaneous potential without incurring an additional significant cost (as is commonly experienced with other development optimization strategies such as increasing hydraulic fractures across the wellbore). The authors also demonstrate through their analysis that economic metrics can improve linearly with increased lateral length while completion design

parameters may be less straightforward since other aspects such as net pay thickness can ultimately limit their increased production potential.

While Britt, Jones, and Miller [2010] illustrate the drilling impact of a 3,000 ft horizontal well in the Barnett shale, it is not uncommon to observe modern horizontal wells extending beyond 1 mile, or 5,280 ft. Chapa [2019] shows that several unconventional wells drilled in Texas have extended beyond 3 miles, with the longest lateral measuring nearly 17,000 ft. Further, 8 out of the top 10 longest horizontal wells were developed in the Permian Basin. The experience that operators and drilling service companies have gained related to this modern development strategy has allowed for increased commercially- and technologically-available reserves. US-EIA [2022] support this through their analysis showing that United States proved reserves of crude oil and lease condensates has more than doubled since 2010 (**Figure 2.3**). This increase in proved reserves is largely backed by onshore field developments, where unconventional reservoirs have become the "industry standard" (Britt, Jones, and Miller [2010]).

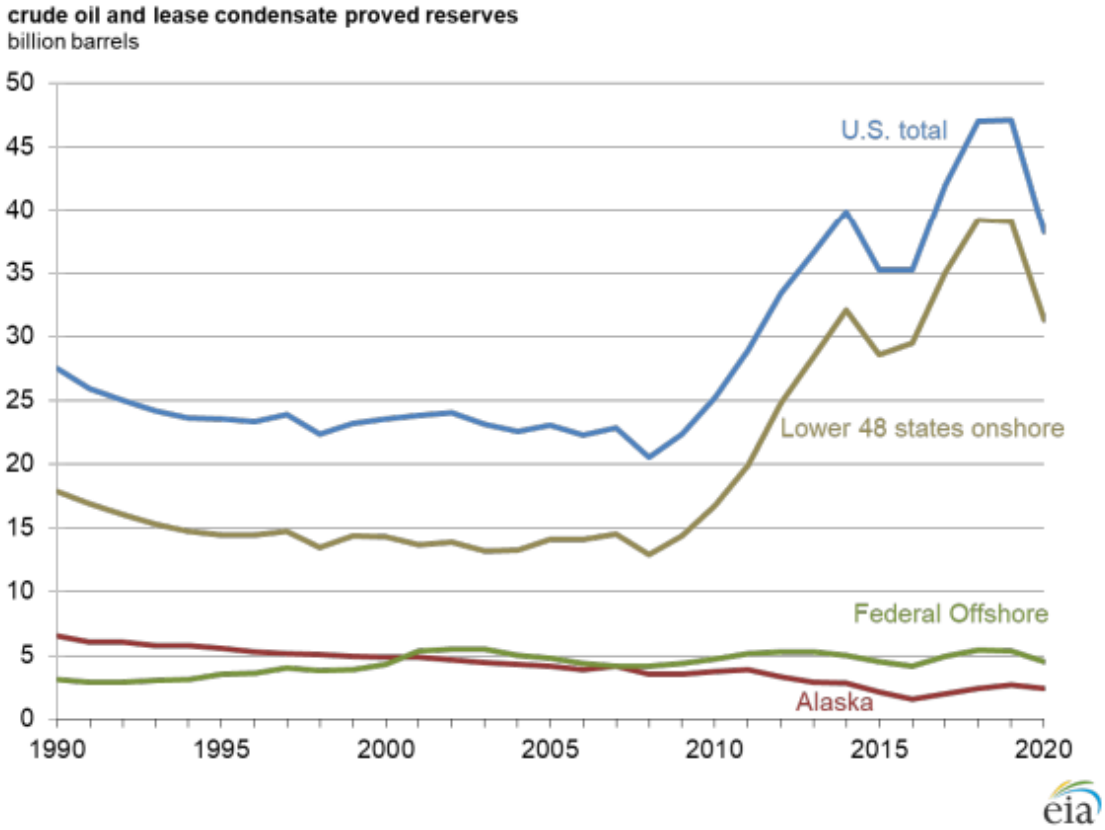

Figure 2.3 — Cartesian plot for the evolution of United States proved crude oil and lease condensate reserves since 1990. Since 2010, the United States has experienced a significant increase in proved reserves, largely supported by the increased utilization of modern horizontal drilling and completion techniques rendering these reserves now commercially available (reprinted from US-EIA, Proved Reserves of Crude Oil and Natural Gas in the United States, Year-End 2020, 2022).

The process of "landing" the lateral section of the wellbore in the reservoir target area, formally called stratigraphic geosteering, is an important part of the drilling process and can drastically influence the ultimate productivity of a well. Saint *et al*. [2014] note that this process is extremely difficult due to varying thicknesses, changing lateral facies, and changing channel geometries commonly encountered. Combinations of measurement-

while-drilling (MWD) and logging-while-drilling (LWD) tools are leveraged to predict the wellbore location at each stage of the drilling process (Saint *et al.* [2014] and Mottahedeh [2008]). Woodward and Noynaert [2017] outline operational considerations related to geosteering and show that pre-drill planning often requires major modifications during the drill process due to the unexpected presence of geologic features ranging from macro-scale fractures to rolling dips near faults. Zhao *et al.* [2022] present advanced methods for collecting stratigraphic reservoir data through the use of ultra-high-definition mapping-while-drilling tools. Zhao *et al.* show that enhanced depth of detection (DOD) and increased anisotropy sensitivity are important in geosteering tools in order to more quickly predict the current drilling environment encountered and improve reservoir encountered rate.

Recently, development of automation processes focused on interpreting real-time geosteering data and guiding engineering decisions has generated a lot of interest (Timonov *et al.* [2021], Heintzelman *et al.* [2022], Santoso *et al.* [2022]). Heintzelman *et al.* [2022] propose an automated geo-correlation algorithm that relies on gamma log calibration to map the actively drilled well to type log from an offset well. Human involvement can be incorporated through the use of "control points" to override any ambiguous interpretations that may occur. Timonov *et al.* [2021] extend the implementation of automated workflows to the pre-drill geosteering planning phase and allow Bayesian models to optimize for the best well landing intervals based on neighboring well log data. Beyond this, the model leverages machine learning methods to forecast production based on the target formation interval and will automatically

correct this geological model using the live log data when drilling operations commence. Santoso *et al.* [2022] outline how a web-based platform leveraging automatic geosteering workflows should be structured in order to maximize effectiveness and collaboration among multiple stakeholders.

Hydraulic Fracturing

While the implementation of certain development strategies (*e.g.*, extending lateral length) can aid in *improving* economics for a well in unconventional or tight formations, only hydraulic fracturing is capable of *rendering* these developments economic (Martin and Rylance [2010]). Hydraulic fracturing is an influential completion technique because it allows for the opening of large surface area in the reservoir rock which provides a conductive path for reservoir fluids to preferentially flow to the wellbore (Ilk [2010]). Various strategies for carrying out hydraulic fracturing operations and stimulating reservoir rock have been documented (Mayerhofer *et al*. [1997]; Walker *et al.* [1998]; Rushing and Sullivan [2003]; Palisch, Vincent, and Handren [2008]). McNeil, van Gijtenbeek, and van Domelen [2012] provide a hydraulic fracture design matrix that guides operator completion strategy based on rock brittleness encountered and personal hydraulic fracture design philosophy (*e.g.*, preference towards fracture intensity, reservoir diversion, or stress-induced complexity). The authors also provide guidance to incorporate natural fracture features in the stimulation treatment planning as these geologic features may significantly control hydraulic fracture propagation and ultimately affect the shape and extent of a well's drainage volume.

Rahman and Gui [2016] show the importance of geomechanical properties (both static and dynamic) when planning stimulation treatment by considering the effects of minimum horizontal stress, pore pressure, and Young's modulus on ultimate hydraulic fracture conductivity, oil production, and net present value. Further, Rahman and Gui highlight that geomechanical modeling can aid in mitigating overflows of water production by properly predicting fracture height growth, thus avoiding overstimulation designs that may penetrate into underlying water-bearing formations. Because the stress orientations may change across the lateral section of the wellbore as each successive fracture stage is completed, 3D discrete fracture network (DFN) models are recommended for confidently predicting fracture growth behaviors and accounting for heterogeneity effects.

Beyond stimulation treatment planning, it is also important that post-stimulation treatment hydraulic fracture efficiency can be confidently evaluated. Cipolla and Wright [2000] develop an extensive overview of currently available tools for hydraulic fracture diagnostics. Both direct and indirect methods for fracture diagnostics are available for operators, but data resolution and costs associated with each method often dictate which are selected in practice.

Microseismic fracture mapping has become a very popular choice for direct, far-field mapping due to its potential in determining fracture length (NOT effective), fracture height, asymmetry, and the azimuth (Cipolla and Wright [2000]). Multiple studies across various basins have illustrated the utility of this technology for multiple purposes (Mayerhofer *et al*. [2005]; Wolhart *et al*. [2005]; Mayerhofer *et al*. [2006]; Cipolla,

Mack, and Maxwell [2010]). Wolhart *et al*. [2005] show that hydraulic fracture length estimates from microseismic data can bound spacing designs for infill wells in order to avoid undesired inter-well communication. Additionally, in depleted sections of a reservoir or where heterogeneity in formation stresses is common, microseismic mapping allows engineers to observe if any stage across the lateral section is dominating hydraulic fracture growth. Cipolla, Mack, and Maxwell [2010] leverage the real-time capability of microseismic data to evaluate stimulation performance on a stage-by-stage basis. Through this process, early detection of insufficient hydraulic fracture stimulation is able to be observed by engineers and the proper corrections to the completion strategy can be addressed at once.

For many operators, indirect methods for fracture diagnostics are preferred in order to avoid additional capital expenditures while developing new wells. Post-stimulation production data analysis, net pressure fracture analysis, and well-testing analysis are commonly incorporated methods for evaluating fracture efficiency indirectly (Barree, Fisher, and Woodroof [2002]; Rushing, Sullivan, and Blasingame [2005]; Nicholson, Hawkes, and Bachman [2019]). Nicholson, Hawkes, and Bachman [2019] note that the diagnostic fracture-injection/falloff test (DFIT) has become the "go-to" method for indirect evaluation of fracture efficiency in unconventional oil and gas resource developments. The DFIT is a well-test analysis that is carried out by characterizing pressure falloff behavior after performing a mini-frac (i.e., injecting sufficient fluid to achieve formation breakdown).

Craig [2017] provides a comprehensive workflow that incorporates DFIT analysis as a method for constraining effective permeability-thickness in a horizontal well, thus, allowing for realistic estimates of fracture conductivity and fracture geometry when performing subsequent history matching and production data analysis. This is an important application of the DFIT since it has been noted by many authors that hydraulic fracture design models have historically overpredicted the amount of effectively stimulated perforation clusters (Ugueto-C. *et al*. [2016]; Wheaton *et al*. [2016]; Haustveit *et al*. [2017]; Somanchi, Brewer, and Reynolds [2017]). Haghshenas and Qanbari [2021] outline how multi-well DFITs can be leveraged to evaluate parent-child effects and to characterize resulting pressure distributions away from wells based on hydraulic fracture preferential growth. Comparing multi-well DFITs to production data analysis of parent wells, Haghshenas and Qanbari also that hydraulic fracture asymmetry and geological heterogeneity effects can be detected.

The integration of DFIT into their analysis provides a method for validating collected pressure and production data associated to parent wells while also addressing the influence pressure depletion may have on the child well hydraulic fracture growth. Recently, developments have been made to improve the structure of the DFIT, with the principal objective being reduced time required for testing (Wang and Sharma [2020]; Zanganeh *et al*. [2020]). Zanganeh *et al*. [2020] show that controlled flowback following a mini-frac can yield similar analysis as DFIT. The key benefit is that testing time must no longer extend to weeks or months waiting for a complete pressure falloff profile. Instead, initial estimates of reservoir pressure and identification of after-closure flow

regimes can be observed on the scale of hours. Zeinabady [2021] also show that rapid evaluations of productivity index can be performed across the lateral section of a horizontal well, while also including perforation friction, tortuosity, and wellbore unloading effects.

2.2. Pressure-Transient Models for Wells Intercepted by Fractures

The study of fluid flow through porous media has been a topic of interest for many years. Improved interpretations of flow behaviors associated with differing reservoir geometries, boundary conditions, and reservoir systems is consistently desired. The purpose of this section is to summarize the logical progression of developments made in well-testing throughout the years to accurately characterize flow behavior in porous media, with a specific focus on the analytical (and semi-analytical) solutions pertaining to wells intercepted by hydraulic fractures.

Fundamental Considerations for Development of Analytical Solutions

Muskat [1946] is a pioneering work that extensively covers the analytical solutions to flow problems related to homogeneous fluids for various reservoir behaviors. The primary method for deriving the analytical solutions in this work is by way of Fourier-Bessel series. van Everdingen and Hurst [1949] show that the Laplace transformation is a preferable method for deriving analytical solutions to flow problems. By eliminating the series expansion requirement associated with Fourier-Bessel series, solutions attained through Laplace transformation are easier to compute and avoid convergence issues. van Everdingen and Hurst outline an additional utility of the Laplace transform when computing the constant terminal rate solution, given the constant terminal pressure

solution, is desired (and vice versa). Leveraging the convenient Laplace transform relationships and the superposition theorem (*i.e.*, Duhamel's principle), direct computation of the alternate terminal condition is possible in the Laplace domain. Due to the convenient Laplace transform relationships that exist, and the reduced complexity Laplace transformations provide to the underlying partial differential equation (*i.e.*, transforming partial differential equation [PDE] to ordinary differential equation [ODE]), this method is heavily favored and implemented when deriving analytical solutions in fluid flow problems.

It is important to note that other analytical methods, capable of providing equivalent quality solutions for complex fluid flow problems, do exist. For example, the development of source functions and Green's functions for varying source and boundary conditions have led to multiple analytical solutions describing the flow behavior for single wells intercepted by vertical (or horizontal) hydraulic fractures in infinite (or bounded) reservoirs (Gringarten and Ramey [1973]; Gringarten and Ramey [1974]; Gringarten, Ramey, and Raghavan [1974]; Gringarten and Ramey [1975]).

Analytical and Semi-Analytical Solutions for Fractured Wells

Gringarten and Ramey [1973] thoroughly review vertical well cases when the reservoir is produced at a prescribed flux (*i.e.*, constant terminal rate). Including Newman's method, Gringarten and Ramey show that complex Green's functions can be developed from the product of simpler Green's functions evaluated at lower dimensions. This development allows for source functions, representative of various reservoir boundary

types, to be generated painlessly while also rendering asymptotic forms of the pressure-drop function readily available.

Gringarten, Ramey, and Raghavan [1974] apply the aforementioned Green's functions and source functions to evaluate a single fracture in a vertical well under uniform flux and infinite conductivity (*i.e.*, constant pressure along the fracture resulting from fluid entry flux) conditions. The uniform flux vertical fracture solution is presented as a first approximation of the infinite conductivity solution and does not require discretization. At very early times, however, the uniform flux solution is exact. Further, the authors show that sampling the uniform flux solution at a particular dimensionless distance value, $x_D = 0.732$, can yield an equivalent infinite conductivity fracture solution.

Gringarten and Ramey [1974] elaborate on the unsteady-state pressure distributions observed when a uniform flux horizontal fracture is created. It is shown that the analytical solution derived is equivalent to the line-source well solution with the addition of skin (Hantush [1957]). Additionally, the authors show that a radius of influence can be defined from the pseudo skin factor. This proxy proves useful for applications related to wells with limited entry or partial penetration.

Cinco-Ley, Samaniego, and Dominguez [1978] extend the work of pressure-transient analysis in fractured wells to the vertical, finite conductivity case. They show through the use of Green's functions and source functions that the unsteady state flow equation can be solved through a rigorous discretization process. Subsequent work would focus

on the analysis of finite-conductivity fractured wells (Cinco-Ley and Samaniego [1981a]; Cinco-Ley and Samaniego [1981b]; Cinco-Ley [1982]).

Larsen and Hegre [1991] present a semi-analytical, discretized approach to solving the horizontal well with finite-conductivity vertical fracture case. The authors solve for wellbore pressure by considering an unbounded 3-D reservoir where the hydraulic fractures may be circular or rectangular in shape. It is shown that boundary conditions may be imposed on the solution through superposition and the concept of images. Chen and Raghavan [1997] present another solution to the multi-fracture horizontal well case. What is more, their solution also takes into account boundary effects, but does not require the method of images. This is accomplished by solving the equation with modern solutions to horizontal wells as is described by Ozkan and Raghavan [1991].

2.3. Pressure-Transient Plotting Functions for Diagnostics

Well Test Derivative

Bourdet, Ayoub, and Pirard [1989] proposed the well testing pressure derivative function, $\Delta p_d(t)$, and showed that when plotted on log-log scale, the infinite-acting radial flow regime was readily identifiable. This development extended the widely-used Horner method and was one of the first methods defined that actively leveraged powerful computing facilities that were becoming available. Many analysts believed that the pressure derivative function provided unique characteristics that conventional type curves did not (Lane, Lee, and Watson [1991]). While the "well testing" pressure derivative function is applicable to cases such as naturally fractured reservoirs, the over-whelming utility of the function lies in evaluating infinite-acting radial flow. During the

radial flow regime, the well testing pressure derivative function (Eq. 2.1) yields a *constant* value.

$$\Delta p_d(t) = \frac{d\Delta p}{d\ln(t)} = t\frac{d\Delta p}{dt} \quad \text{..... (2.1)}$$

where:

Δp = Pressure difference

t = Time

Several authors (*e.g.*, Bourdet, Ayoub, and Pirard [1989]; Bryan, Ilk, and Blasingame [2021]; Escobar, Navarrete, and Losada [2004]) have noted that computation of the "Bourdet" well testing derivative can magnify noise in the underlying pressure derivative, particularly at the endpoints. Smoothing algorithms are available to mitigate this challenge, but the question of "how much smoothing is acceptable" is still unclear.

Alternative approaches to computing well test derivatives have been proposed. Lane, Lee, and Watson [1991] and Escobar, Navarrete, and Losada [2004] proposed the use of splines as an approximation of the pressure derivative however this process requires considerable user input for computation. Fulford and Blasingame [2020] attempted to resolve this issue by proposing the use of Bayesian statistics to evaluate derivative functions after an outlier filtering algorithm is performed. While still requiring filtering before evaluation, the authors noted that no assumptions regarding the data distribution are needed.

Pressure Integral

Blasingame, Johnston, and Lee [1989] had a novel approach to plotting functions that actually integrated well test data instead of differentiation (Eq. 2.2). This approach yielded smoother type curves in their well test analyses consisting of vertically-fractured wells. Onur, Peres, and Reynolds [1989] also published a pressure integral function for well test analysis and developed a relationship between the pressure function and well drainage area.

$$p_{Di} = \frac{1}{t_D}\int_0^{t_D} p_D(\tau)\,d\tau \quad \text{..... (2.2)}$$

where:

p_{Di} = Dimensionless pressure integral

p_D = Dimensionless pressure

t_D = Dimensionless time

τ = Variable of integration

Beta-Derivative

Hosseinpour-Zonoozi, Ilk, and Blasingame [2006] improved upon the original definition of the β-derivative plotting function, $\Delta p_{\beta d}(t)$, by Sowers [2005] (*i.e.*, Eq. 2.3 below). Hosseinpour-Zonoozi, et al can be of great utility in cases exhibiting strong power-law behavior (*e.g.*, fractured wells, horizontal wells, boundary detection) (see **Fig. 2.4**).

$$\Delta p_{\beta d}(t) = \frac{d\ln(\Delta p)}{d\ln(t)} = \frac{1}{\Delta p} t \frac{d\Delta p}{dt} = \frac{\Delta p_d(t)}{\Delta p} \quad \text{..... (2.3)}$$

Through the development of Eq. 2.3 Hosseinpour-Zonoozi, et al also identified a relationship with the "cartesian" pressure derivative (given by Eq. 2.4). This pressure derivative function was previously studied by Mattar and Zaoral [1992] and was referred to as the "primary pressure derivative" in their work.

$$\Delta p_{pd}(t) = \frac{d\Delta p}{dt} \quad \text{..... (2.4)}$$

Hosseinpour-Zonoozi, Ilk, and Blasingame [2006] presented an exhaustive analysis of type curves which included the implementation of the β-derivative for diagnostics. As a result of their work, they identified the β-derivative characteristic response for an array of relevant reservoir and well cases (**Table 2.1**). While the authors did provide sample analysis for the reservoir heterogeneity case, this was limited to the case of a dual porosity reservoir with pseudosteady-state interporosity flow.

Chow Pressure Group

Chow [1952] illustrated the utility of pressure derivative ratios as plotting functions for transmissibility determinations pertaining to artesian aquifers. Several authors have implemented this concept, which is commonly referred to as the "Chow pressure group", in their studies of pressure data (Ozkan [1988]; Flamenco-Lopez and Camacho-Velazquez [2003]; Chu *et al.* [2017]; Ballinger *et al.* [2022]). Ozkan [1988] included the Chow pressure group (CPG) as presented in Eq. 2.5 in his analysis of wellbore storage influences on horizontal well and vertically fractured well responses.

$$\Delta p_{CPG} = \frac{\Delta p}{2\dfrac{d\Delta p}{d\ln(t)}} = \frac{\Delta p}{2t\dfrac{d\Delta p}{dt}} = \frac{\Delta p}{2\Delta p_d(t)} \quad \text{..... (2.5)}$$

Chu *et al.* [2020] incorporated the Chow pressure group in their work as a proxy for magnitude of interference between two wells. Their work was aimed at developing a relationship between the Chow pressure group and standalone well estimated ultimate recovery (EUR).

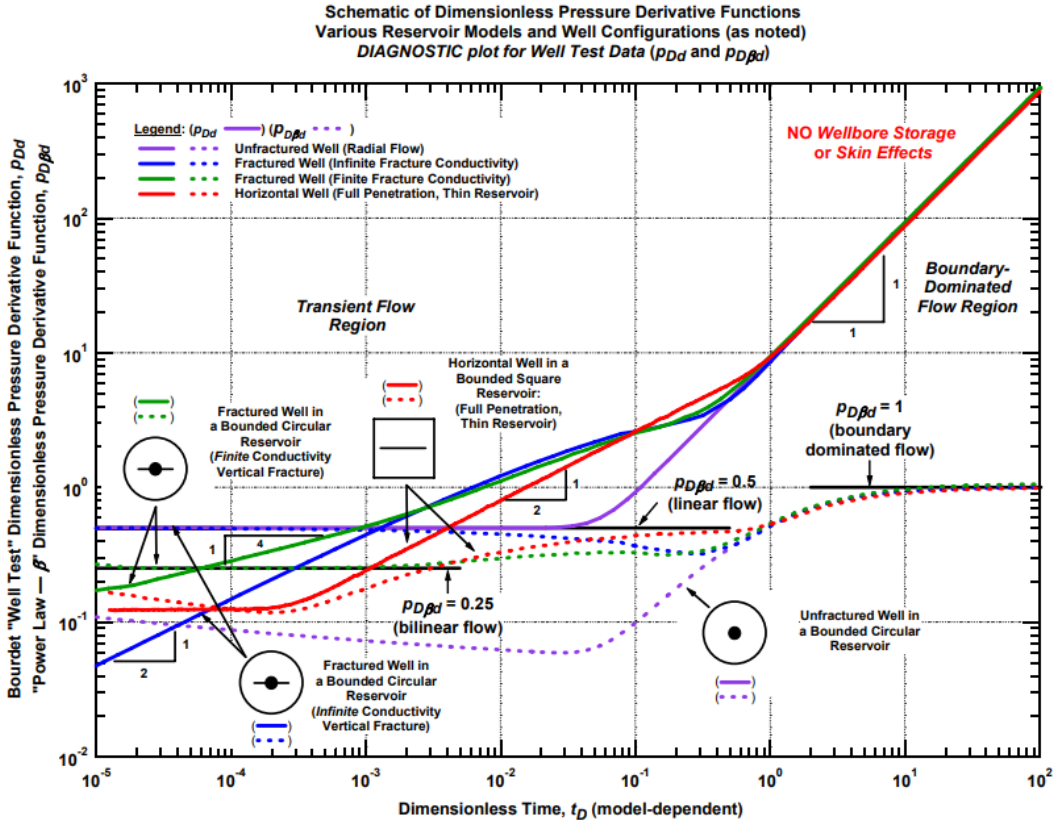

Figure 2.4 — Log-log plot serving as a schematic diagnostic plot illustrating the well testing pressure derivative and β-derivative plotting functions for varying well types and reservoir boundary conditions. Power-law flow behaviors show as constant values able to be immediately read from diagnostic plot (reprinted from Hosseinpour-Zonoozi, Ilk, and Blasingame [2006], SPE-103204-MS).

Table 2.1 — Summary of β-derivative characteristic behaviors for relevant well and reservoir cases (recreated after Hosseinpour-Zonoozi, Ilk, and Blasingame [2006], SPE-103204-MS)

Case	$\Delta p_{\beta d}(t)$
• Wellbore storage domination:	1
• Reservoir boundaries:	
— Closed reservoir (circle, rectangle, etc.).	1
— 2-Parallel faults (large time).	1/2
— 3-Perpendicular faults (large time).	1/2
• Fractured wells:	
— Infinite conductivity vertical fracture.	1/2
— Finite conductivity vertical fracture.	1/4
• Horizontal wells:	
— Formation linear flow.	1/2

CHAPTER III

TRILINEAR FLOW MODEL FOR EVALUTATING RESERVOIR PERFORMANCE IN UNCONVENTIONAL SHALES*

In this section we introduce the trilinear flow model as a practical method for evaluating reservoir performance in unconventional shale reservoirs. We present an overview of the model assumptions and discuss the model symmetry that is exploited when deriving the analytical solution. Following this, we generate a series of type curves that illustrate the effect different phases of the reservoir system have on the overall pressure-transient solution. Finally, we apply the trilinear flow model to field data we have obtained as a result of both pressure buildup (PBU) and pressure drawdown (PDD) tests.

3.1. Model Foundation

The practical pressure-transient model that we have identified in this work is the trilinear flow model (Brown *et al*. [2011]). This model exploits the concept of symmetry and simplifies computation requirements by focusing on one "symmetry element" across the horizontal well and solving for its pressure-transient behavior. **Figure 3.1** is presented to illustrate the symmetry element modeled. We note that this element is exactly the region between two planar, hydraulic fractures and extends from the horizontal wellbore to the outer reservoir boundary, denoted by x_e. With this serving as the symmetry

*The following URTeC paper, *Application of the β-Derivative to Evaluate Multi-Fractured Horizontal Well Performance in Unconventional Shale Reservoirs*, is reprinted with permission from the Unconventional Resources Technology Conference, whose permission is required for further use.

element, the total pressure response for the multi-fracture horizontal well can be evaluated through a simple scale-up methodology.

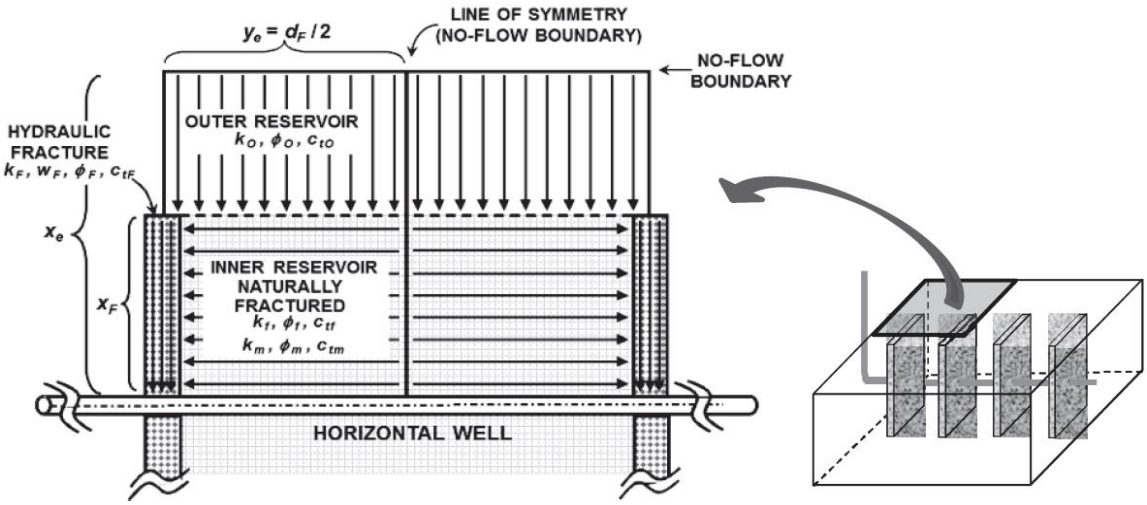

Figure 3.1 — Schematic diagram for the symmetry element used in the development of trilinear flow model for evaluating reservoir and hydraulic fracture performance of a multi-fracture horizontal well in unconventional shale reservoirs (reprinted from Brown *et al*. [2011]).

Beyond the use of a symmetry element, the trilinear flow model assumes that there are three distinct regions where flow occurs, and that when combined, can represent the total reservoir-well system for a multi-fracture horizontal well. These three flow regions are:

- Outer reservoir.
- Inner reservoir.
- Hydraulic fractures.

By defining these three flow regions, Brown *et al* simplify the development of an analytical solution since they can now solve for each region and couple the solutions through the careful consideration of boundary conditions. It is important to note that

these three flow regions allow the authors to also simplify flow within each region to be linear in behavior. Beginning with the outer reservoir, flow is linear into the inner reservoir region. Once in the inner reservoir region, flow is assumed linear into the hydraulic fractures. This flow into the hydraulic fractures occurs along the fracture half-length, and thus, is in a direction perpendicular to flow into the inner reservoir from the outer region. Once flow enters the hydraulic fracture, it is connected to the horizontal wellbore and only through the fractures can production occur. Additionally, no flow enters the hydraulic fracture through the fracture tips, only along the fracture half-length.

To highlight the different flow regions that the multi-fracture horizontal well model is comprised of under the trilinear flow methodology, we present the Laplace transformed partial differential equations that govern flow within the outer reservoir, inner reservoir, and hydraulic fractures, respectively:

$$\frac{\partial^2 \bar{p}_{OD}}{\partial x_D{}^2} - \frac{s}{\eta_{OD}} \bar{p}_{OD} = 0 \quad \text{..... (3.1)}$$

$$\frac{\partial^2 \bar{p}_{ID}}{\partial y_D{}^2} + \left(\frac{1}{y_{eD} C_{rD}} \right) \frac{\partial \bar{p}_{OD}}{\partial x_D}\bigg|_{x_D=1} - u\bar{p}_{ID} = 0 \quad \text{..... (3.2)}$$

$$\frac{\partial^2 \bar{p}_{fD}}{\partial x_D{}^2} + \frac{2}{C_{fD}} \frac{\partial \bar{p}_{ID}}{\partial y_D}\bigg|_{y_D=w_{fD}/2} - s\bar{p}_{fD} = 0 \quad \text{..... (3.3)}$$

Incorporating the boundary conditions that couple the three flow regions together, the final analytical solution for dimensionless wellbore pressure is the following:

$$\bar{p}_{wD} = \frac{\pi}{C_{fD} s \sqrt{\alpha_f} \tanh\left(\sqrt{\alpha_f}\right)} \quad \text{..... (3.4)}$$

We encourage consultation of the Brown *et al*. reference[2011] for further details related to solving the partial differential equations presented in Eqs. 3.1-3.3. A key advantage of the trilinear flow model is the direct capability of modeling reservoir heterogeneity in the inner reservoir region. Because the completion process associated with multi-fracture horizontal wells can often times significantly alter rock stresses and induce natural fractures, it is important that this reservoir heterogeneity can be captured in pressure-transient models. Avoiding complex discrete fracture models requiring large amount of computing power, idealized dual porosity models are used instead. Through the use of the transfer function in the Laplace space, $f(s)$, both pseudosteady state dual-porosity and transient dual-porosity natural fractures can be incorporated. With our work focused on the transient behavior of unconventional shale reservoirs, we utilize the transient dual-porosity model in our analysis after Serra *et al*. [1983]. It should be noted that the definitions associated with the dual porosity model parameters do differ depending on if the flow behavior is transient or pseudosteady state. To avoid confusion, we provide the *transient* dual porosity model definitions as follows:

$$\omega = \frac{\left(\phi c_t\right)_m}{\left(\phi c_t\right)_{nf}} \quad \text{..... (3.5)}$$

$$\lambda = 12\left(\frac{l^2}{h_m{}^2}\right)\left(\frac{k_m h_m}{k_{nf} h_{nf}}\right) \quad \text{..... (3.6)}$$

3.2. Development of Type Curves

With the foundations of the trilinear flow model established, we now generate type curves to highlight the influence of flow regions on the overall pressure solution. The

reservoir and hydraulic fracture parameters provided in Brown *et al*. [2011] serve as the base inputs as we begin generating our type curves. For convenience, the diagnostic plots that we provide for all type curves are presented in dimensionless form. A full log of type curves generated from this work is available in **Appendix A**.

Hydraulic Fracture Conductivity

Figures 3.2-3.5 present dimensionless type curves for four cases of dimensionless hydraulic fracture conductivity (*i.e.*, C_{fD} = 1, 10, 100, 1000) with wellbore storage effects also included. In each figure, early wellbore storage domination is present and is detectable when the β-derivative value is equal to unity. Next, the β-derivative pressure function captures very clearly the effects of the hydraulic fracture conductivity as the flow regime transitions from early-time effects to the fracture flow and transient dual porosity flow regimes.

We note that the larger hydraulic conductivity cases exhibit greater "dips" in the β-derivative during transition flow regions, while the lower conductivity cases are less pronounced. As expected, the lower conductivity cases exhibit a β-derivative value closer to one-fourth, while the higher conductivity cases are near one-half. Consulting **Table 2.1**, this is not a surprise since lower conductivity fractures present bilinear flow and higher conductivity fractures present linear flow characteristics.

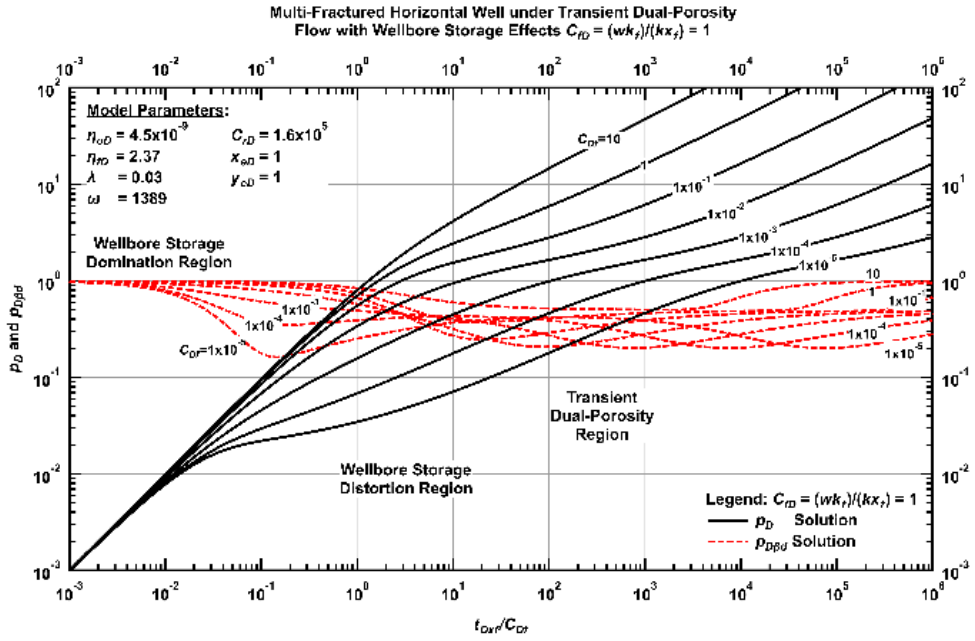

Figure 3.2 — Log-log scale diagnostic plot for a multi-fracture horizontal well in transient dual porosity reservoir (C_{fD} = 1).

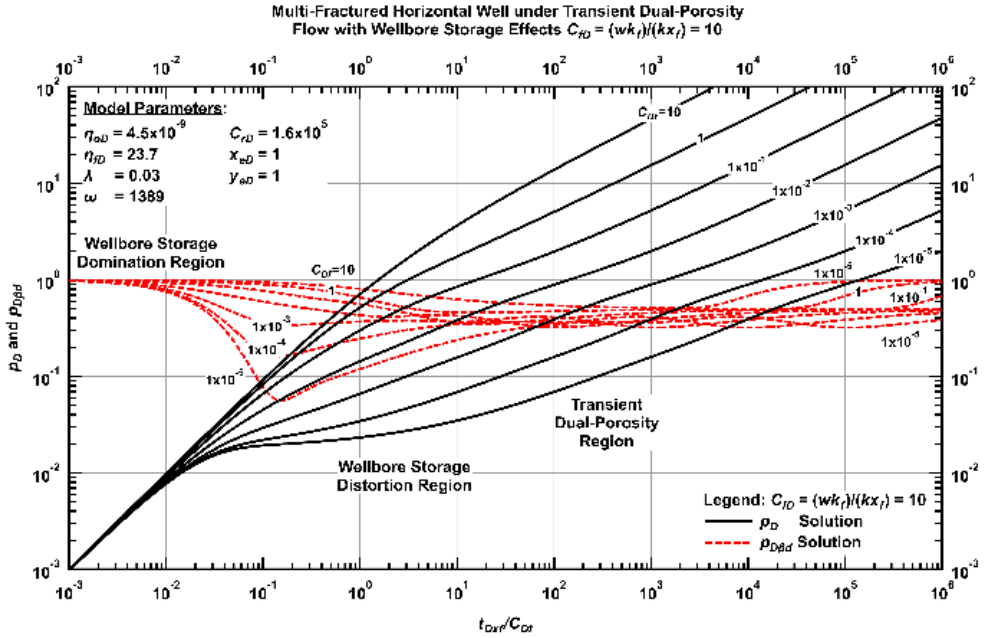

Figure 3.3 — Log-log scale diagnostic plot for a multi-fracture horizontal well in transient dual porosity reservoir (C_{fD} = 10).

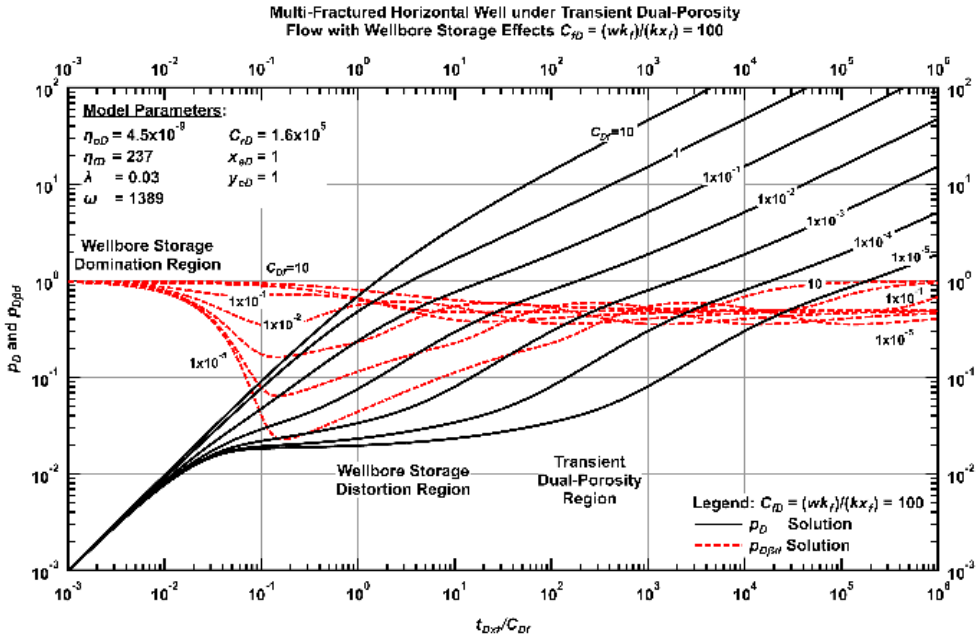

Figure 3.4 — Log-log scale diagnostic plot for a multi-fracture horizontal well in transient dual porosity reservoir (C_{fD} = 100).

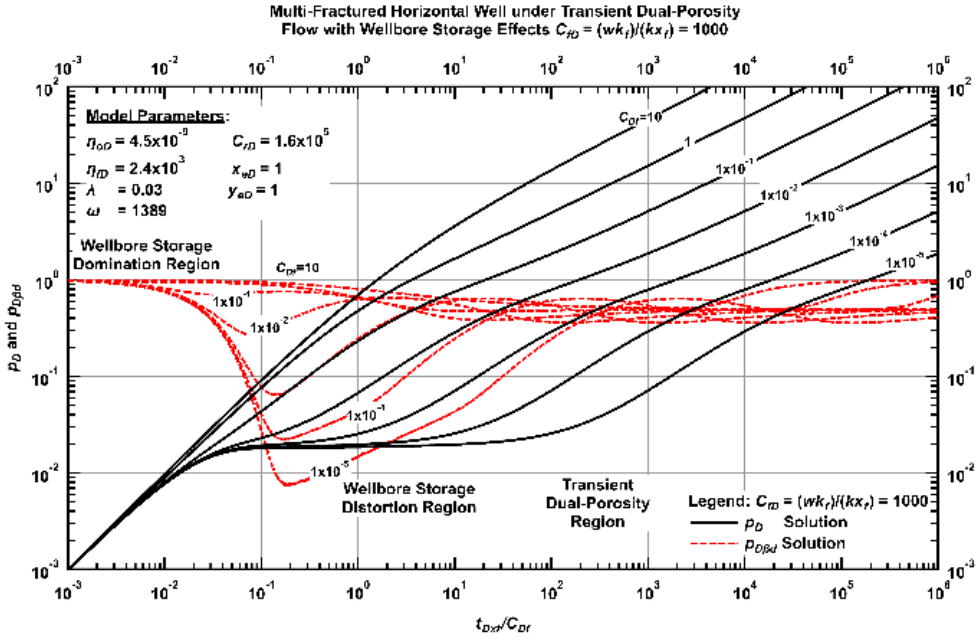

Figure 3.5 — Log-log scale diagnostic plot for a multi-fracture horizontal well in transient dual porosity reservoir (C_{fD} = 1000).

Transient Flow-Capacity Ratio

We recall the definition for the transient flow-capacity ratio for the dual porosity model:

$$\lambda = 12\left(\frac{l^2}{h_m{}^2}\right)\left(\frac{k_m h_m}{k_{nf} h_{nf}}\right) \quad \text{..... (3.6)}$$

As commentary, we note that the flow-capacity ratio is also referred to as the interporosity flow coefficient. No difference in the definitions arise as long as it is understood whether the transient or pseudosteady state condition is being implemented. Next, we define a grouping parameter for our convenience that will allow us to combine wellbore storage effects and dual porosity effects in a simplified, controllable manner:

$$\alpha = \lambda C_{Df} \quad \text{..... (3.7)}$$

Finally, we now select three unique "alpha" values that we will use to generate type curves modeling wellbore storage and natural fracture influences (*i.e.*, $1x10^{-4}$, $1x10^{-1}$, and $1x10^{2}$). **Figures 3.6-3.8** present the type curves generated for these grouping parameter values. We note that the dimensionless wellbore storage coefficients involved in these type curves range from $1x10^{-5}$ to $1x10^{3}$ in order to give a complete representation of the analytical solutions. For each of the type curves presented, we ensure that hydraulic fracture conductivity is held constant equal to 250. Thus, as flow regime transitions from wellbore storage to flow within the stimulated reservoir volume occur, direct comparisons across different values of transient flow-capacity ratios are possible.

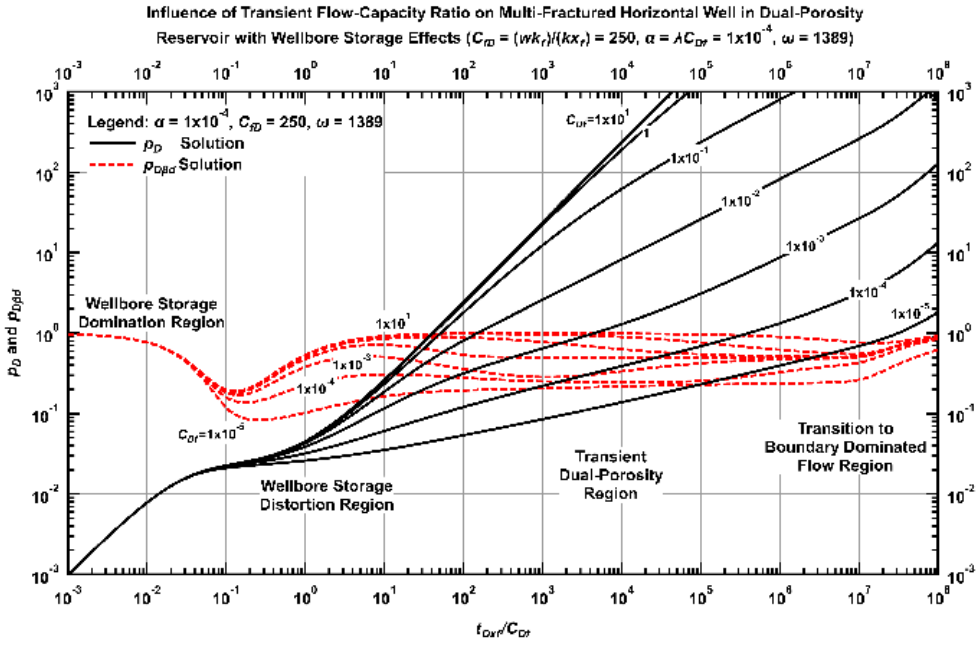

Figure 3.6 — Log-log scale diagnostic plot for a multi-fracture horizontal well in transient dual porosity reservoir (α = 1x10^{-4}).

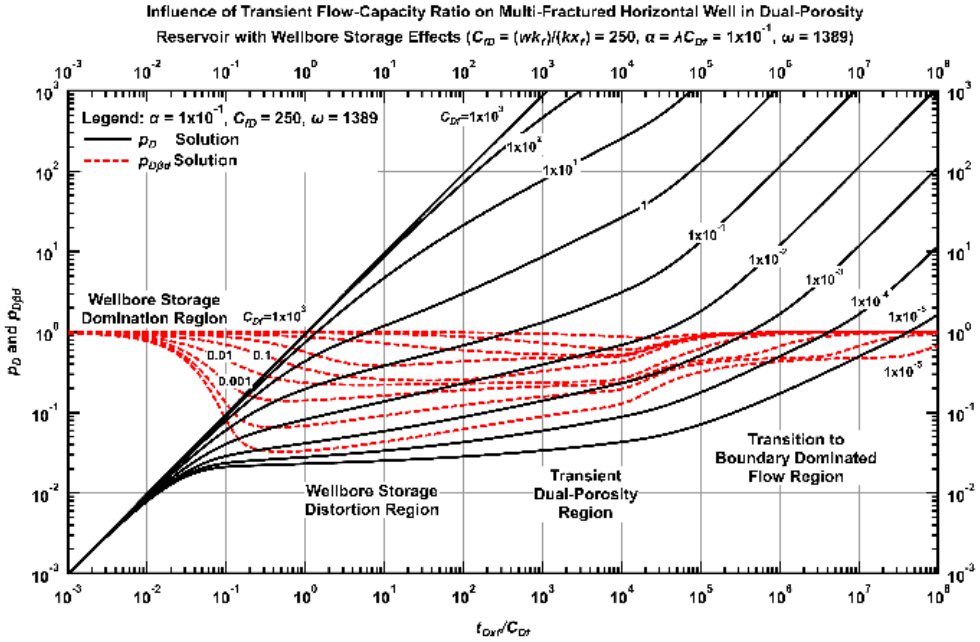

Figure 3.7 — Log-log scale diagnostic plot for a multi-fracture horizontal well in transient dual porosity reservoir (α = 1x10^{-1}).

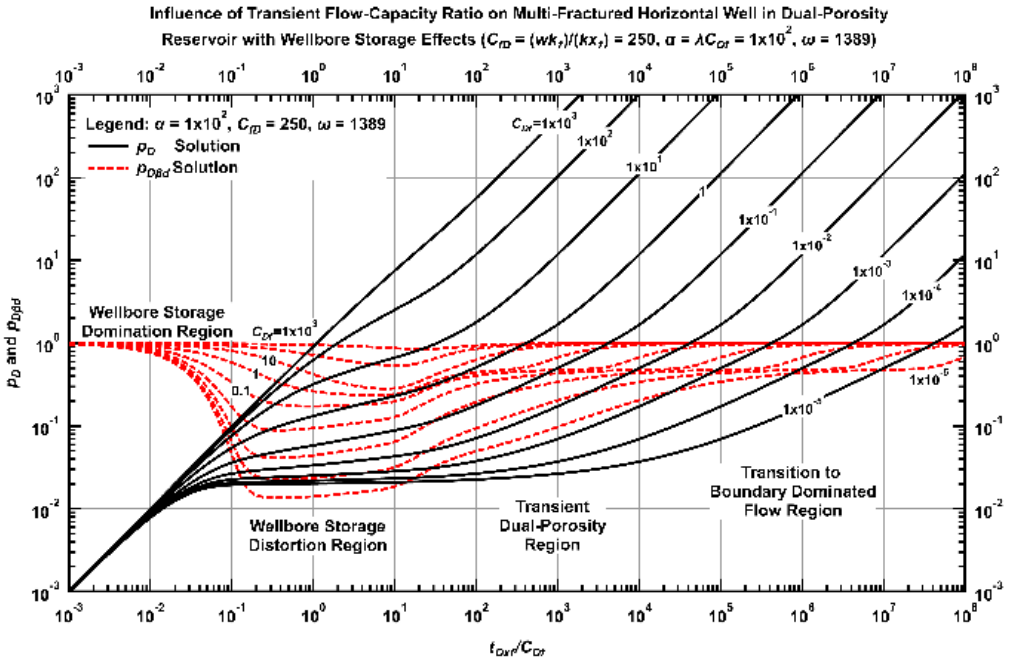

Figure 3.8 — Log-log scale diagnostic plot for a multi-fracture horizontal well in transient dual porosity reservoir ($\alpha = 1x10^2$).

When values for the transient flow-capacity ratio decrease, indicative of less conductive natural fractures, the β-derivative value also decreases. This is a convenient observation since it is very similar to the characteristic behavior seen amongst hydraulic fractures of varying conductivity. As the α value is increased, which in turn generally coincides with an increased transient flow capacity ratio, the transition flow region can persist for multiple log-cycles. This behavior can be identified upon inspection of the β-derivative. The region where the β-derivative is changing (*i.e.*, not relatively constant or "flat") can provide evidence that a specific flow regime has not been firmly established or is not present in the analysis. This direct approach to identifying flow regimes and transition flow regions is one of the principal advantages of the β-derivative.

3.3. Applications to Field Data

In this section we apply the trilinear flow model to two field data cases received. We note that all three cases were from multi-fracture horizontal wells that exhibit typical fluid properties, well parameters, and completion designs as commonly seen from Permian Basin oil wells.

Pressure Buildup Test

Figure 3.9 presents the pressure buildup profile for Well #4 after being shut-in for 74 hours. Although a relatively short test, the pressure buildup exhibits a relatively "smooth" profile. Using this pressure buildup test, we generate a diagnostic plot from the data and include our fitted model (**Figure 3.10**). A schematic of the well and fracture geometry used to generate the trilinear flow model solution is provided by **Figure 3.11**.

We present this pressure buildup case to highlight the commonly-observed features for a multi-fracture horizontal well in unconventional shale reservoirs. From early-time, we note that the well is dominated by wellbore storage (confirmed by the β-derivative value equal to unity). Following this flow regime, a transition to a strong, power law flow region is observed. While this is not uncommon for wells that exhibit fracture-dominated flow periods, we observe that the β-derivative does not stabilize at a value of one-fourth or one-half. Instead, the β-derivative stabilizes to a value near seven-tenths. To match this mid-time behavior, we tune our natural fracture model parameters as is seen from the in-plot summary results.

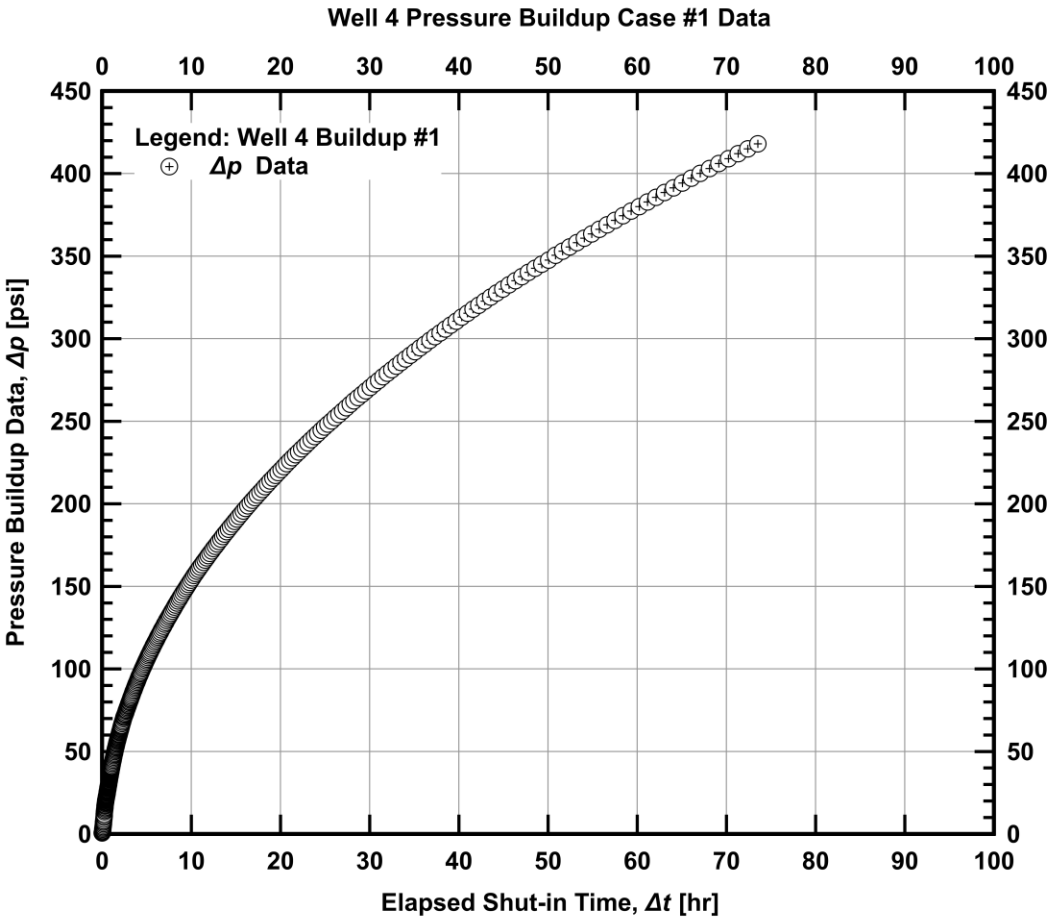

Figure 3.9 — Cartesian scale plot illustrating the pressure buildup profile attained as a result of Well #4 being shut-in for 74 hours.

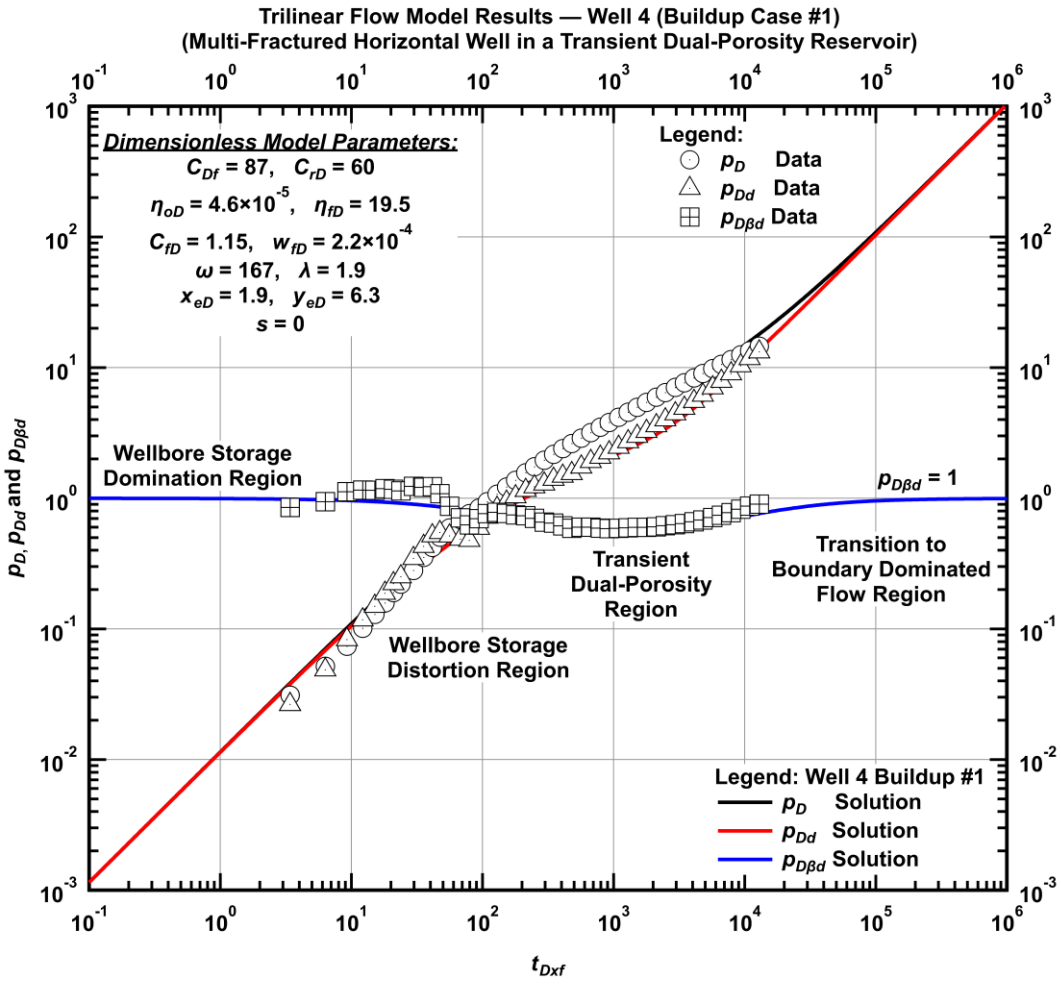

Figure 3.10 — Log-log scale diagnostic plot for Well #4 pressure buildup case #1 including the fitted trilinear flow model solution. From this case we note the early-time wellbore storage domination and the typical power-law flow regime exhibited at mid-time when the well experiences fracture-dominated flow characteristics.

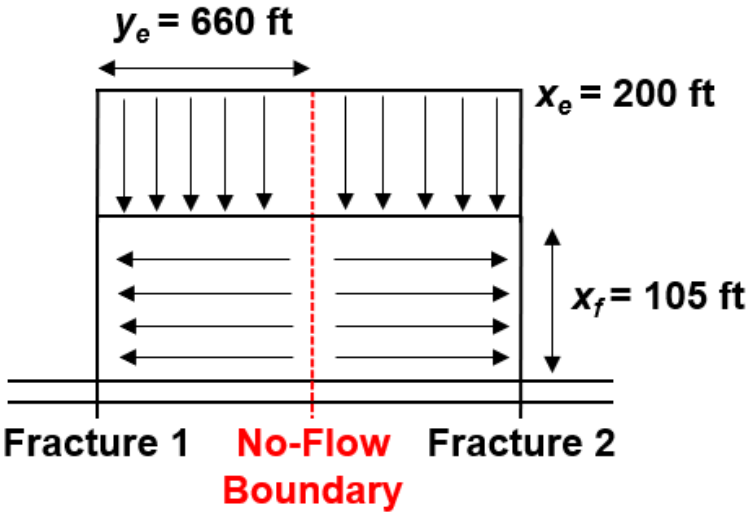

Figure 3.11 — Schematic diagram for the well and hydraulic fracture geometry parameters required to generate the trilinear flow model match for Well #4 PBU case #1.

Upon inspecting the well and hydraulic fracture geometry parameters required to generate a fitted trilinear flow model solution, we note that the estimated distance between two hydraulic fractures is overly-large. It would not make practical sense for the hydraulic fractures to be spaced this wide. With this said, however, this could possibly be an indication that the *efficiency* (or conductivity) of the hydraulic fractures is not great.

This short pressure buildup case highlights some of the main flow regime features that may be expected for wells in unconventional shale reservoirs. Additionally, the rigor required for well test analysis is illustrated by observing the long amount of time that would be required to see anything beyond fracture-dominated flow.

Pressure Drawdown Test

The second field data analysis is related to a pressure drawdown test conducted over 257-hours for Well #1. **Figures 3.12** and **3.13** present the pressure buildup profile and diagnostic plot, respectively, for the pressure drawdown test. **Figure 3.14** illustrates the well and hydraulic fracture geometry parameters required to generate the trilinear flow model solution.

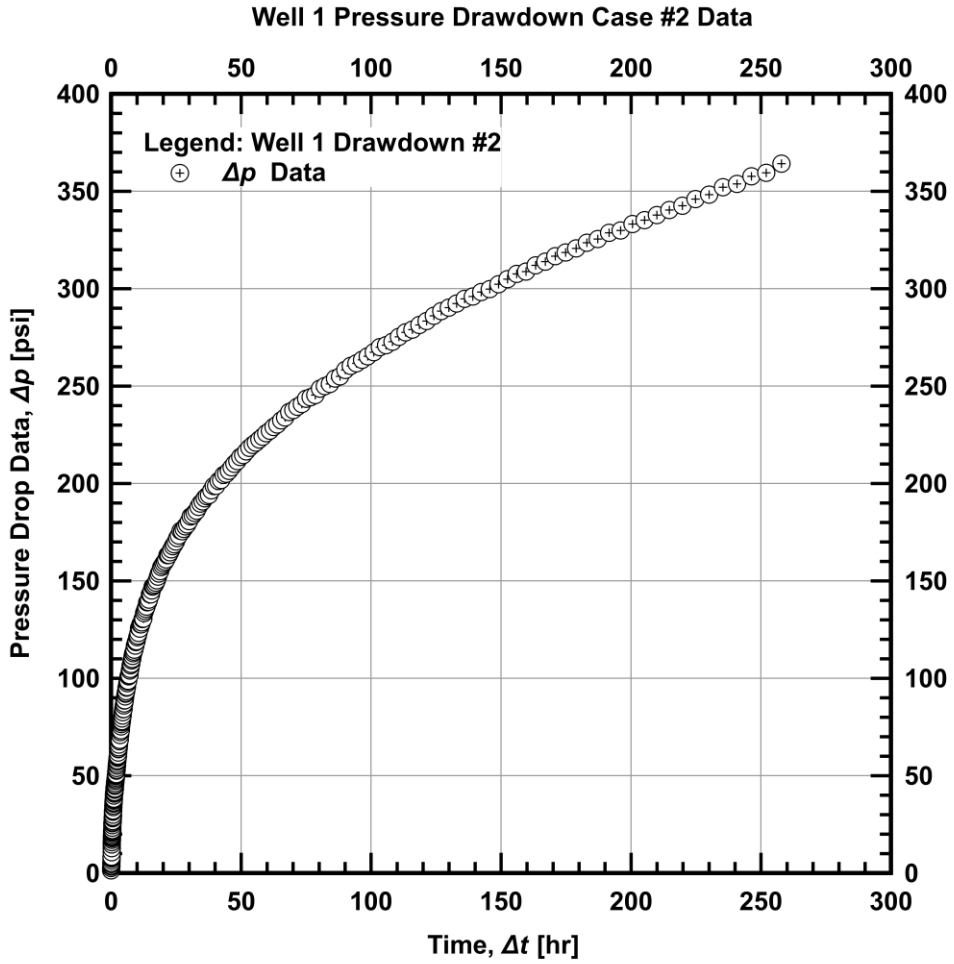

Figure 3.12 — Cartesian scale plot illustrating the pressure drawdown profile attained as a result of Well #1 being under drawdown for 257 hours.

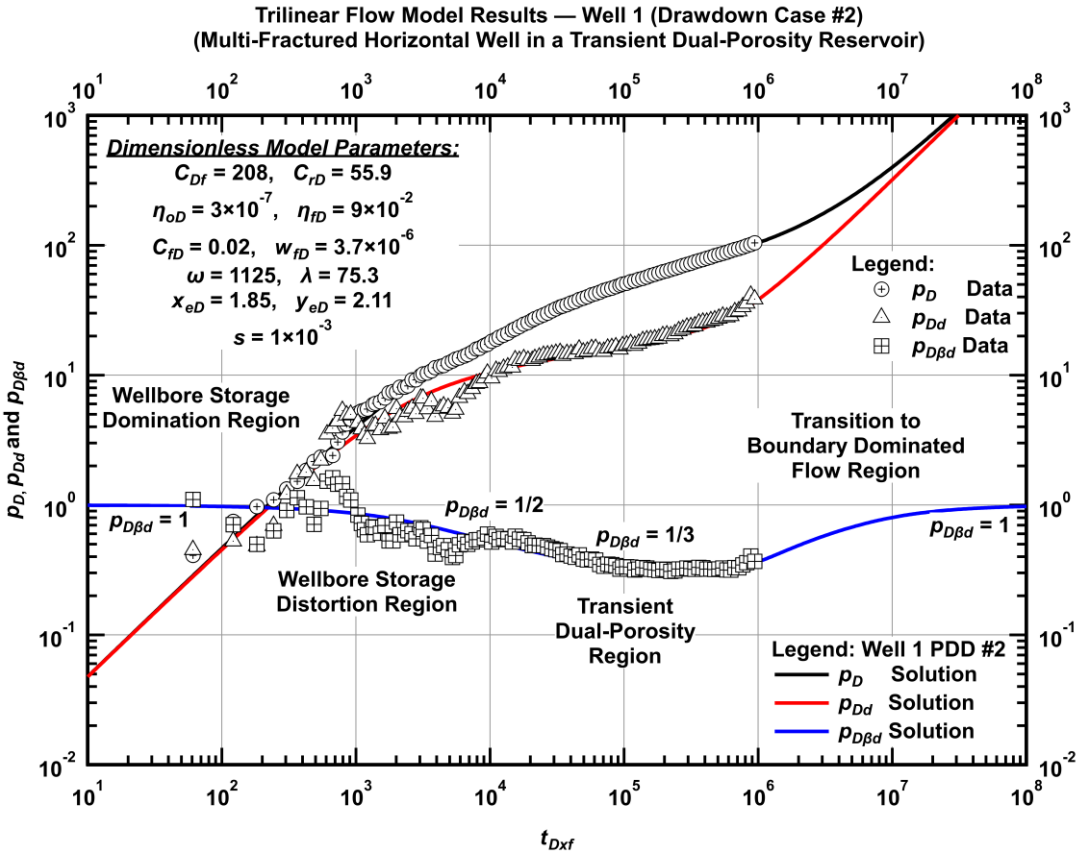

Figure 3.13 — Log-log scale diagnostic plot for Well #1 pressure drawdown case #1 including the fitted trilinear flow model solution. From this case we note the early-time wellbore storage distortion and the two regions where stabilized β-derivative values occur at mid-time.

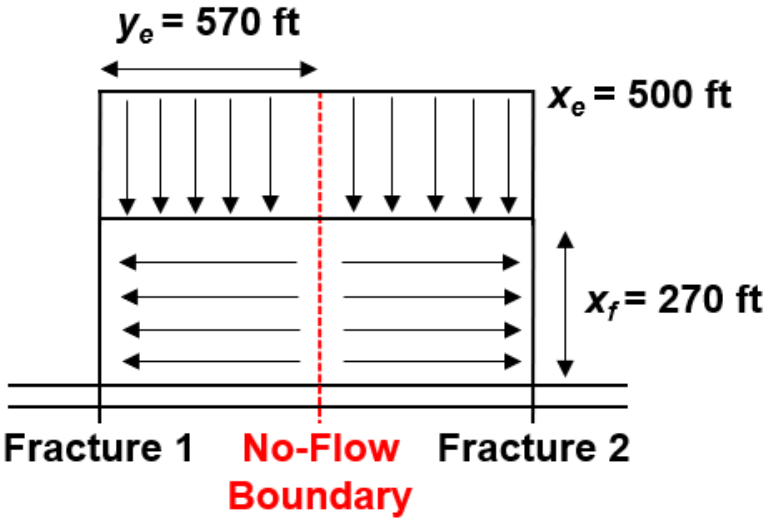

Figure 3.14 — Schematic diagram for the well and hydraulic fracture geometry parameters required to generate the trilinear flow model match for Well #1 PDD case #2.

From the diagnostic plot we note that the well exhibits early-time wellbore storage distortion effects. The β-derivative is helpful in identifying the proper wellbore storage coefficient needed for our model match. With this set as a "lock", we now focus on the power-law flow regimes associated with fracture-dominated flow. We note that at a dimensionless time value near $1x10^4$ a brief region with a stabilized β-derivative value is observed. The value at this point is near 1/2, which we would expect from a high conductivity hydraulic fracture. However, after some time a transition flow regime occurs and we identify another stabilized region, this time with a β-derivative value near 1/3. This region of stabilized flow extends for a little over 1 log-cycle.

In order to generate a model match, we require the hydraulic fracture have a half-length equal to 270 ft. On its own, an effective fracture half-length of this magnitude would indicate an effective stimulation treatment. However, we note again that the hydraulic fracture spacing is quite large compared to what we expect for a horizontal well. Due to the two stabilized β-derivative flow regions we observe, it is possible that the hydraulic fractures have variable conductivity. We recall that due to the simplified nature of the trilinear flow model in this respect, we are not able to reflect different hydraulic fracture properties across the lateral wellbore. This is due to the implementation of a symmetry element.

If additional information were available beyond the pressure data, further analysis could be carried out to confirm or reject whether variable fracture conductivity is a possibility. Completion records would be useful in gathering a holistic view of the horizontal well and its performance. Nevertheless, these two examples still stand to outline the methodology that can be readily applied to well test data when leveraging a practical model like the trilinear flow model. Additionally, strategic incorporation of auxiliary pressure functions like the β-derivative provide unique characteristics that can aid in diagnostic work.

CHAPTER IV

APPLICATION OF THE BETA DERIVATIVE AS A DIAGNOSTIC TOOL FOR WELL AND FRACTURE INTERFERENCE ANALYSIS

In this section we introduce a numerical multifracture horizontal well model (MFHW) including both a "parent" and "child" well. We simulate two cases of interference that can be commonly encountered in practice. The first case varies the hydraulic fracture spacing across the horizontal well to observe hydraulic fracture interference (*i.e.*, "fracture-to-fracture" interference). The second case varies the well spacing between parent and child well to observe well interference (*i.e.*, "well-to-well" interference). The overall effects of these interference events are analyzed. Additionally, the β-derivative is included in the diagnostic plot analysis and serves as a tool for identification of interference events.

4.1. Development of the Two-Well Numerical Model

Grid Description

A single layer reservoir of thickness equal to 130 feet and depth to reservoir top equal to 8,000 feet serves as the basis for our numerical analysis. Using commercial software, we implement a polygonal grid geometry with refined grids near the wells and between the individual hydraulic fractures. An important feature that we include in our grid description are non-coarsened grids at the location of the child well. Without explicit selection of this option, the default choice results in coarser grids around the well not being actively analyzed (*i.e.*, the child well). Failure to refine grids in this area will

result in a lower resolution computation of pressure distributions and may not sufficiently capture the propagation of the pressure front as the well produces. It should be noted that this selection to model more descriptively the non-analyzed well provides detailed description of the pressure behavior between hydraulic fractures, however, the computational time will obviously increase.

Table 4.1 outlines the number of computed grids for each simulation run conducted throughout this analysis. Qualitatively, the increase in computation resources required for each run is appreciated by comparing the total number of grid blocks solved for each time-step. Naturally, the simulation cases with a higher density of hydraulic fractures across the horizontal well (*i.e.*, a "tighter" fracture spacing) require further discretization in the stimulated reservoir volume (SRV) and results in more grid blocks being included. This is confirmed by evaluating the percent change in the number of grid blocks, based to the widest hydraulic fracture spacing case. Further observation of the grid block percentage change column shows that the number of grid blocks generated is not directly proportional to number of hydraulic fractures modeled. Taking the "tightest" hydraulic fracture spacing scenario (53-foot spacing) as example, we note that the percentage change for the grid blocks is 247.0%. The associated percent change for the number of hydraulic fractures (from 5 to 20 fractures) is 300%. In this case *the number of grid blocks did not increase as much as the number of hydraulic fractures*.

Table 4.1 — Summary table for total number of grid blocks included for each simulation case analyzed for both varying hydraulic fracture spacing scenarios and varying well spacing scenarios.

Case	n_{grid}	Δn_{grid} (%)
• Hydraulic Fracture Spacing Sensitivities:		
— 250-foot fracture spacing (n_f = 5)	10,326	—
— 167-foot fracture spacing (n_f = 7)	15,986	54.8
— 111-foot fracture spacing (n_f = 10)	22,214	115.1
— 53-foot fracture spacing (n_f = 20)	35,834	247.0
• Well Spacing Sensitivities:		
— 800-foot well spacing (n_f = 5)	10,333	—
— 700-foot well spacing (n_f = 5)	10,349	0.15
— 500-foot well spacing (n_f = 5)	10,342	0.09
— 400-foot well spacing (n_f = 5)	10,326	-0.07
— 300-foot well spacing (n_f = 5)	10,208	-1.21

Well spacing does not appear to affect the number of grid blocks generated as significantly as hydraulic fracture spacing. We note that most of the simulation cases performed required less than a 1% change in number of grid blocks, with only the 300-foot well spacing case having a 1.21% percent change resulting in *less* grid blocks generated. We believe that this reduction in grid blocks is due in part to the wells nearly touching at their respective fracture tips (only 100-feet separate them), thus not requiring a repeated discretization outside of the fractures for both wells. **Figure 4.1** presents a representation of our two well reservoir model.

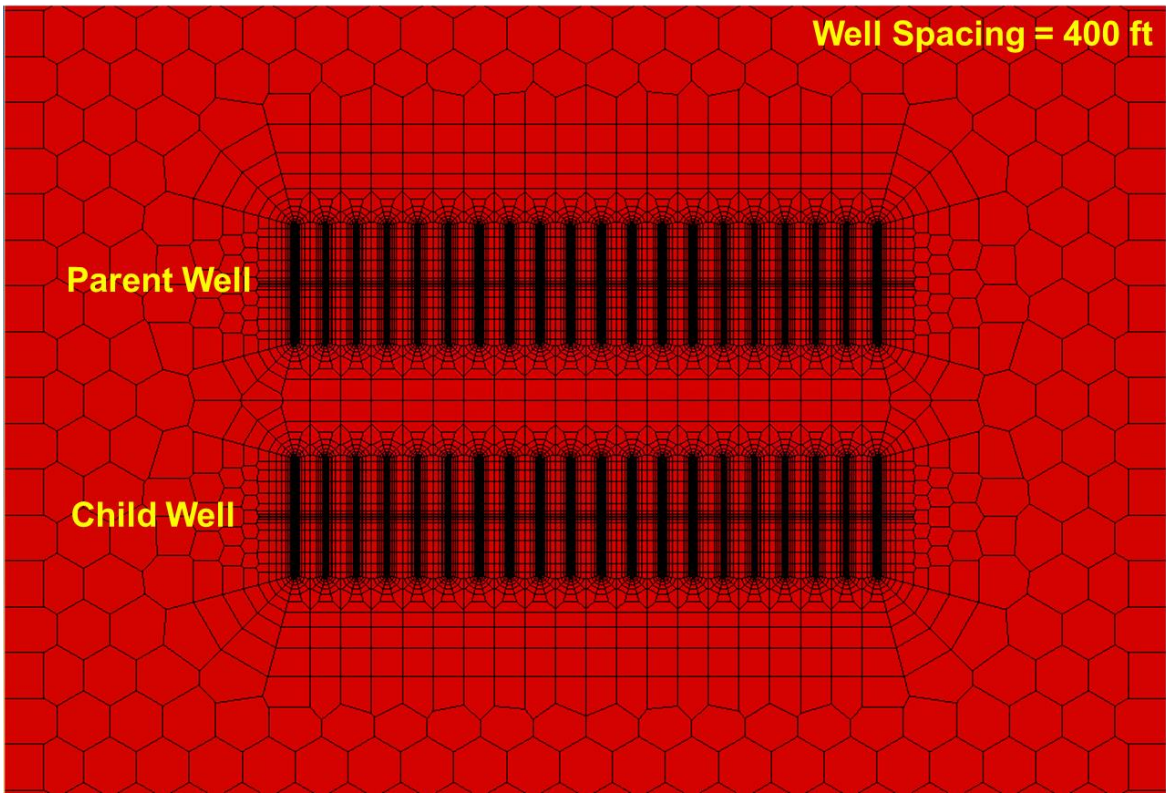

Figure 4.1 — Example reservoir and well model for an infill development scenario. Provided example illustrates a 400-ft well spacing design with hydraulic fractures spaced 53-ft apart (*i.e.*, 20 hydraulic fractures evenly distributed across a 1000-ft well).

Reservoir, Fluid, and Operating Properties

Table 4.2 is presented as a summary for all reservoir, fluid, and operating properties used in the development of the two well numerical model. Kuuskraa, Oudinot, and Koperna [2019] provide a comprehensive analysis of all parameters and properties required for performing reservoir simulation in the Wolfcamp Shale Bench B, and accordingly, we follow many of their PVT and reservoir descriptions in this work.

In order to capture both depletion and interference effects in an efficient manner, we choose to model our reservoir system with an augmented formation permeability as compared to Kuuskraa, Oudinot, and Koperna. The formation permeability value we utilize is 0.05 millidarcy. In practice, based on acreage location within the Wolfcamp Shale Bench B, formation permeability may be on the order of 200 nanodarcy (0.0002 millidarcy).

Concerning the rock units present in the Wolfcamp Shale Bench B, we limit our study to the organic shale rock unit. We acknowledge that further analyses including the organic shale and mixed lithology rock units would aid in capturing heterogeneity effects in reservoir simulation studies. However, with the main intent for our work being related to proving the effectiveness of pressure (and derivative) plotting functions for interference analysis, the homogeneous approach of modeling the organic shale rock unit is appropriate. As such, we assume the formation compressibility is 2.2×10^{-5} psi^{-1}, porosity is uniform and equal to 5%, and the oil saturation is equal to 75%.

Table 4.2 — Reservoir, fluid, and operating properties for well interference modeling case — idealized hydraulically fractured horizontal well with properties and parameters adapted after the Wolfcamp Shale Bench B.

Reservoir Properties:

Net pay thickness, h	=	130 ft
Formation permeability, k	=	0.05 md
Wellbore radius, r_w	=	0.3 ft
Formation compressibility, c_f	=	2.2 x 10^{-5} psi^{-1}
Porosity, ϕ	=	0.05 (fraction)
Initial reservoir pressure, p_i	=	4265 psia
Oil saturation, S_o	=	0.75 (fraction)
Skin factor, s	=	0.00 (dimensionless)
Wellbore storage coefficient, C_s	=	0.01 (bbl/psi)
Reservoir temperature, T_r	=	159 °F

Fluid Properties:

Oil gravity, °API	=	39
Gas-Oil-Ratio, GOR	=	850 scf/stb
Gas specific gravity, γ_g	=	0.7 (air = 1)
Water specific gravity, γ_w	=	1.0 (water = 1)

Hydraulically Fractured Well Model Parameters:

Fracture half-length, x_f	=	100 ft
Fracture conductivity, F_C	=	5000 md–ft
Number of fractures, n_f	=	5 (will vary)
Fracture spacing, d_f	=	250 ft (will vary)
Base case well spacing, d_w	=	400 ft (will vary)
Horizontal well length, L_w	=	1000 ft

Production Parameters:

<u>*Parent Well*</u>

First Producing Time, $t_{p,1}$	=	5760 hr
First Producing Rate, q_1	=	50 stb/d
Second Producing Time, $t_{p,2}$	=	2208 hr
Second Producing Rate, q_2	=	0 stb/d (shut-in)

<u>*Child Well*</u>

First Producing Time, $t_{p,1}$	=	5808 hr
First Producing Rate, q_1	=	0 stb/d
Second Producing Time, $t_{p,2}$	=	2160 hr
Second Producing Rate, q_2	=	50 stb/d (put-on-production)

For fluid composition, the oil gravity is set equal to 39 °API with an associated gas-oil-ratio of 850 scf/STB. Gas and water specific gravities are initialized to 0.7 and 1.0, respectively. We note that this fluid description is initialized for a constant reservoir temperature of 159 °F and an initial, uniform reservoir pressure of 4265 psia.

The proposed hydraulic fracture model is uniform and consists of multiple planar hydraulic fractures across a 1000-ft horizontal wellbore. To investigate hydraulic fracture interference, four scenarios of hydraulic fracture spacing are simulated (53, 111, 167, and 250 feet between fractures). When investigating well interference effects, the hydraulic fracture spacing remains constant and equal to the "wide" spacing scenario (250 feet). For each scenario simulated, the hydraulic fracture spacing is equal across the entire lateral section. Each hydraulic fracture half-length is 100 feet and its conductivity is maintained at 5000 md-ft.

The operating conditions imposed for the two-well multi-fracture horizontal well model follows the shut-in prior-producing approach commonly observed in parent-child cases. Put simply, we allow the parent well to continuously produce from the reservoir for eight months (5760 hours) at a surface production rate equal to 50 STB/D. Upon 5760 hours of production, the parent well is shut-in and 2 days (48 hours) of no changes are simulated. This period of no activity is leveraged later in the analysis for estimations of the power-law exponent with respect to the parent well. After 48 hours of stabilization, the child well is brought online (begins production) at constant surface production rate equal to 50 STB/D. The child well is allowed to produce at this rate for 3 months. This

operating schedule is maintained constant for each of the six well spacing scenarios simulated (300, 400, 500, 600, 700, and 800 feet).

4.2. Hydraulic Fracture Spacing Effects on Interference

Diagnostic Plot Analysis

Figure 4.2 outlines the pressure buildup profiles generated for each of the four hydraulic fracture spacing scenarios as observed from the shut-in prior-producing parent well in a standard "diagnostic plot" format.

We note the following key features from the presented diagnostic plot:

- Early-time wellbore storage distortion is present in the region where the β-derivative transitions away from a value near unity.
- Strong, power-law flow regimes are observed by analyzing the linear pressure functions and the stabilized horizontal β-derivative function at intermediate time.
- Detection of hydraulic fracture interference becomes apparent at late-time and is more pronounced for the "tighter" spaced hydraulic fracture scenarios.

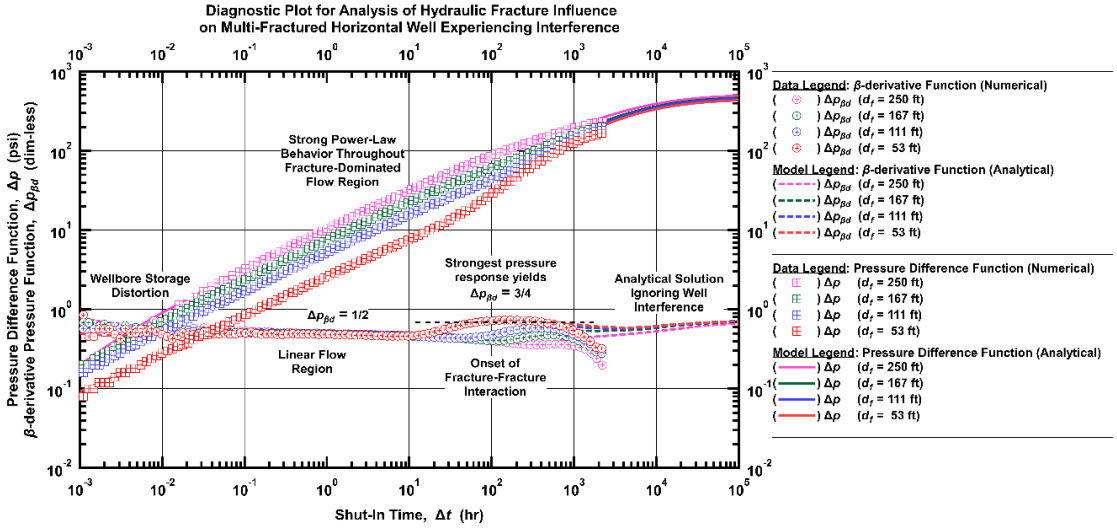

Figure 4.2 — Log-log scaled diagnostic plot illustrating the influence of hydraulic fracture spacing during a pressure buildup test for a prior-producing shut-in multi-fractured horizontal well.

With our prescribed wellbore storage constant not being relatively large (0.01 bbl/psi) the period of wellbore storage domination is not significant and is not observed from the diagnostic plot. We maintain a non-zero value of wellbore storage in our numerical analysis however to illustrate the flow characteristics associated with the transition between early-time flow regimes. As expected, a fracture-dominated flow regime is established very soon after wellbore storage distortion. More precisely, we observe a linear flow region, which is consistent with our created hydraulic fracture model that included a fracture conductivity value equal to 5000 md-ft. During this region we note that the β-derivative is constant and equal to 1/2.

Finally, as time evolves, interference between the planar hydraulic fractures ensues. Naturally, the tighter hydraulic fracture spacing scenarios detect interference earlier.

The 53-ft hydraulic fracture spacing scenario detects the most significant amount of interference and is noticed upon observation of the β-derivative around 100 hours of shut-in time. Interference is observed and a new β-derivative value appears to begin stabilize (approximately equal to 3/4). For a brief period of time, for this tightest hydraulic fracture spacing scenario, it appears that the pressure distributions created by the hydraulic fractures stabilize and begin acting as a combined system. Directly after this period, well interference becomes significant between the parent and child well and the β-derivative begins to "rollover" and decline. Hydraulic fracture interference is appreciable in the other spacing scenarios as well, however, these effects occur at later time and do not fully-stabilize to yield a new β-derivative value.

For comparative purposes, for each of the hydraulic fracture spacing scenarios, we include the associated single-well analytical solution for the parent well assuming that the child well was never developed nor produced. We choose to include this model to allow for comparisons of well interference from both the pressure functions and the β-derivative functions. As expected, the analytical solution matches the data from early- to mid-time perfectly. However, it is only when the influence of the child well begins to be detected that the analytical and numerical solutions diverge (at $\approx$1000 hours shut-in time).

Cartesian Plot Analysis

We include **Figure 4.3** in our analysis to show the effects of pressure interference on a cartesian scale. It should be noted that we utilize elapsed time in this scenario out of preference, but the time may be re-scaled by subtracting the total production time of the parent well (5760 hours) from the provided range of elapsed time, *t*.

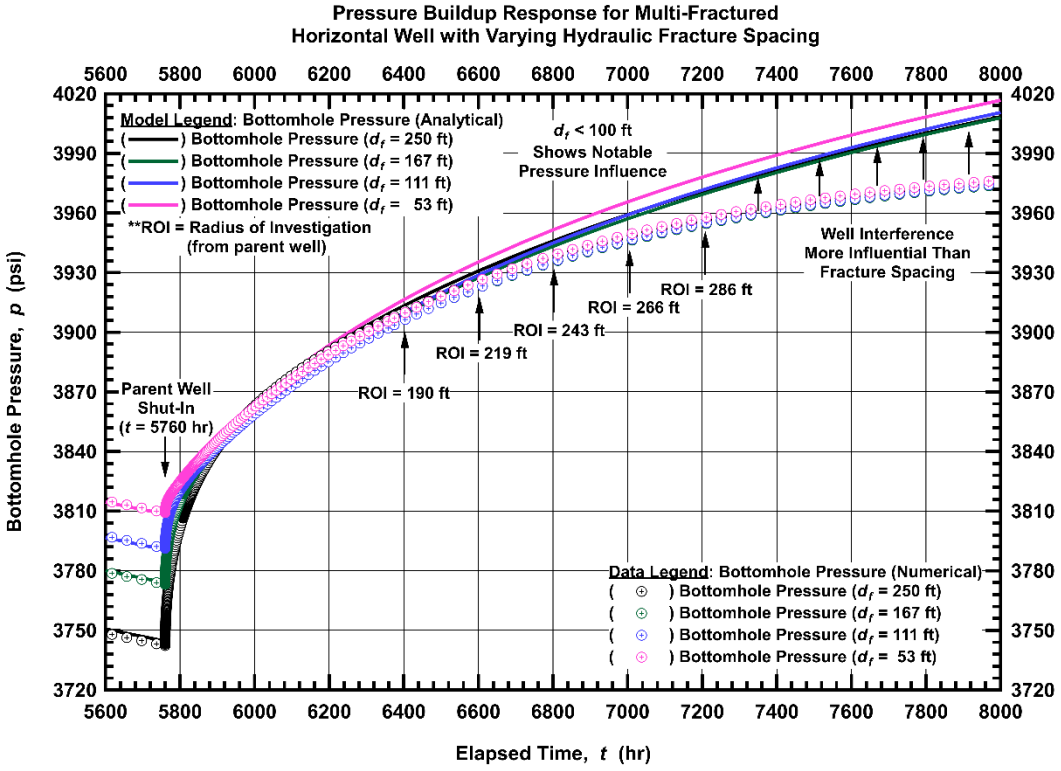

Figure 4.3 — Cartesian scale plot illustrating the pressure buildup profiles for a multi-fracture horizontal well experiencing pressure interference effects due to differing hydraulic fracture spacing designs. Notable difference in pressure response is noticed for the tightest hydraulic fracture spacing (d_f = 53 ft). Well interference resulting from the child well being put on production proves more influential for this sensitivity analysis (all cases model parent well 400 ft away from child well).

We include the averaged radius of investigation (from the parent well) calculated by commercial software for specified times throughout the pressure buildup profile for context. It should be noted that the "ellipse of interference" as described by Lee, Rollins, and Spivey [2003] is an alternative approach for estimating the distance to pressure front for scenarios involving hydraulic fractures. However, for simplicity, the simplified radius of investigation concept is leveraged in this example.

Beginning at the time of shut-in (t = 5760 hours), we note that the tighter hydraulic fracture spacing scenarios yield a greater bottomhole pressure. Because tighter hydraulic fracture spacing is analogous to more hydraulic fractures in this case, less pressure drawdown is required to achieve the pre-established constant surface production rate target. Therefore, it is logical that the 250-ft hydraulic fracture spacing case should have the lowest bottomhole pressure at the time of the parent well shut-in.

As the parent well begins its pressure buildup for each hydraulic fracture spacing scenario, there is minimal difference between each numerical result. However, as time evolves beyond 6200 hours of total elapsed time, it becomes apparent that the numerical results and the analytical results diverge. Referencing the averaged radius of investigation (ROI) values provided, we see that at 6400 hours of elapsed time the estimated ROI approaches 190 ft. Considering that the hydraulic fracture half-length for each well modeled is 100 ft and the controlled well spacing is maintained at 400 ft, the approximate distance between the hydraulic fracture tips is 200 ft. Thus, it can be inferred that this is the time upon which well interference becomes more influential than

the hydraulic fracture spacing. Focusing our attention on the region between parent well shut-in and onset of well interference (5760-6400 hours) we note that there is slight pressure buildup differences, but this is limited to approximately 20 psi for most scenarios. Therefore, we conclude that while a pressure difference is observed due to hydraulic fracture spacing differences, the overwhelming interference observed is due to the child well.

We summarize from this discussion that hydraulic fracture interference is apparent but requires implementation of the diagnostic plot and incorporation of auxiliary plotting functions such as the β-derivative to appreciate its full character.

Connecting the β-derivative to the Power-Law Exponent

While we have shown the utility of the β-derivative in terms of identifying pressure interference as it relates to hydraulic fracture spacing (and well spacing to an extent). The β-derivative also intrinsically provides advantages related to power-law flow regimes for both pressure-transient and rate-transient analysis. To illustrate this advantage, we present **Figure 4.4**.

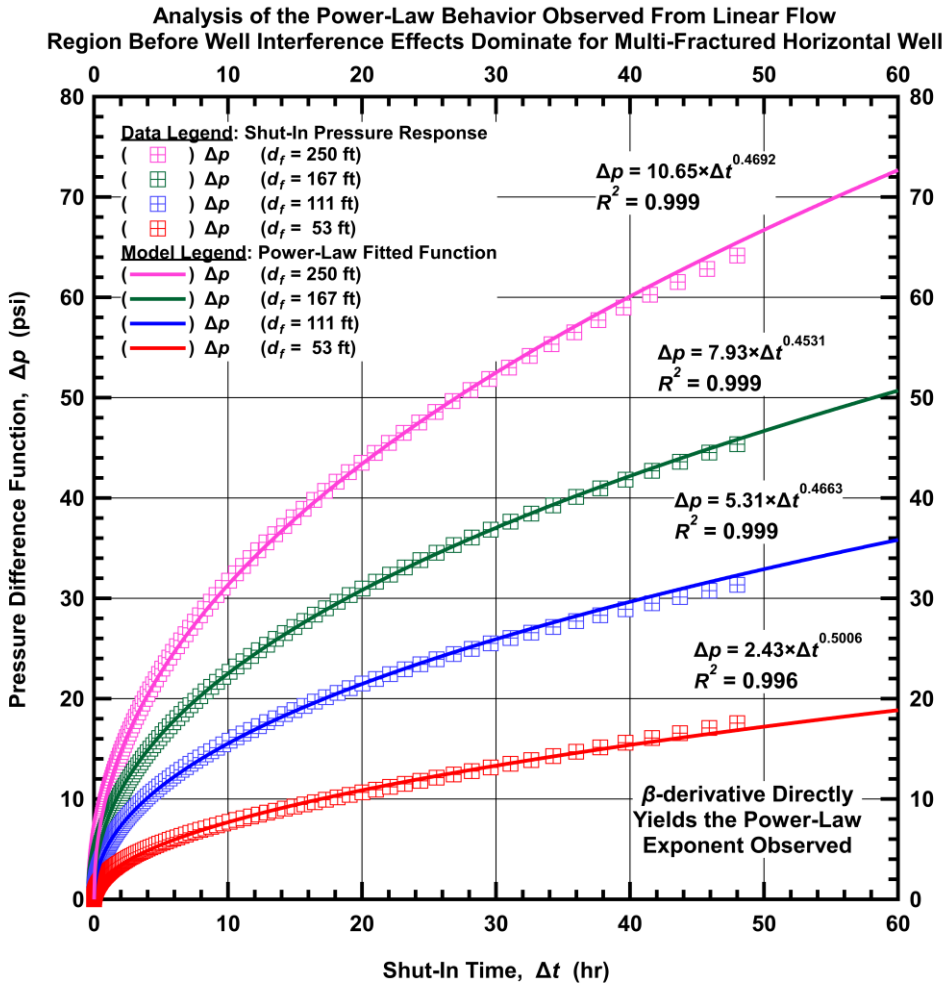

Figure 4.4 — Cartesian scale plot for the pressure buildup profiles of each hydraulic fracture spacing scenario simulated. Data is provided for the first 48 hours of parent well shut-in before the child well is put on production to avoid well interference effects. Power-law trendlines are fitted through regression analysis to illustrate the utility of the β-derivative as a means to directly estimate the pressure behavior and identify associated power-law flow regimes.

Recalling that a strategic 48-hour shut-in period for stabilization purposes is performed before the child well is put on production, we can analyze a portion of the parent well buildup profile before any well interference effects interrupt. Due to our expectation of strong, power-law flow regimes in the early-time region of a pressure buildup (and as confirmed by the diagnostic plot provided in **Fig. 4.2**) it is logical that a general power-law function should reasonably "fit" our numerical data results.

Using a simple regression algorithm, a power-law function is fit to each of the hydraulic fracture spacing scenarios. We note excellent regression analysis for each of the hydraulic fracture spacing scenarios, with all regressions maintaining a coefficient of determination (*i.e.*, R^2) greater than 0.995. However, of particular interest for reservoir engineers is the power-law exponent associated with each of these fitted power-law trendlines. What we observe is that *each power-law exponent is very close to* 0.5, *or* 1/2. This is not a coincidence. In fact, this is the "slope" of the pressure functions for a well that is undergoing a linear flow region. This value is also directly inferred from the β-derivative. The β-derivative helps to identify the underlying fluid flow characteristics associated with various power-law flow regimes is a clear advantage and why we adopt the use of the β-derivative in this work.

4.3. Well Spacing Effects on Interference

To interpret the well spacing effects on interference we perform six numerical simulations for varying well spacing scenarios (300, 400, 500, 600, 700, and 800 feet). We then conduct our analysis of interference by observing the pressure buildup profile using a diagnostic plot. Finally, for the well spacing of 800 feet, we also include a "desuperposition" analysis to interpret interference.

Diagnostic Plot Analysis

Figure 4.5 is presented to show the effects of well spacing on the pressure functions when plotted on a diagnostic plot.

We note the following key features from **Fig. 4.5**:

- Neither wellbore storage domination nor wellbore storage distortion is detected at shut-in times as early as $1x10^{-1}$ hour.
- Stabilized, linear flow regime is established at very early-times and extends for multiple log cycles.
- All well spacing scenario results match identically from early-time through intermediate-time, only differing at late-time (Δt > 200 hours).
- The β-derivative function captures late-time well interference effects very well and is evident when the derivative function begins to decline.

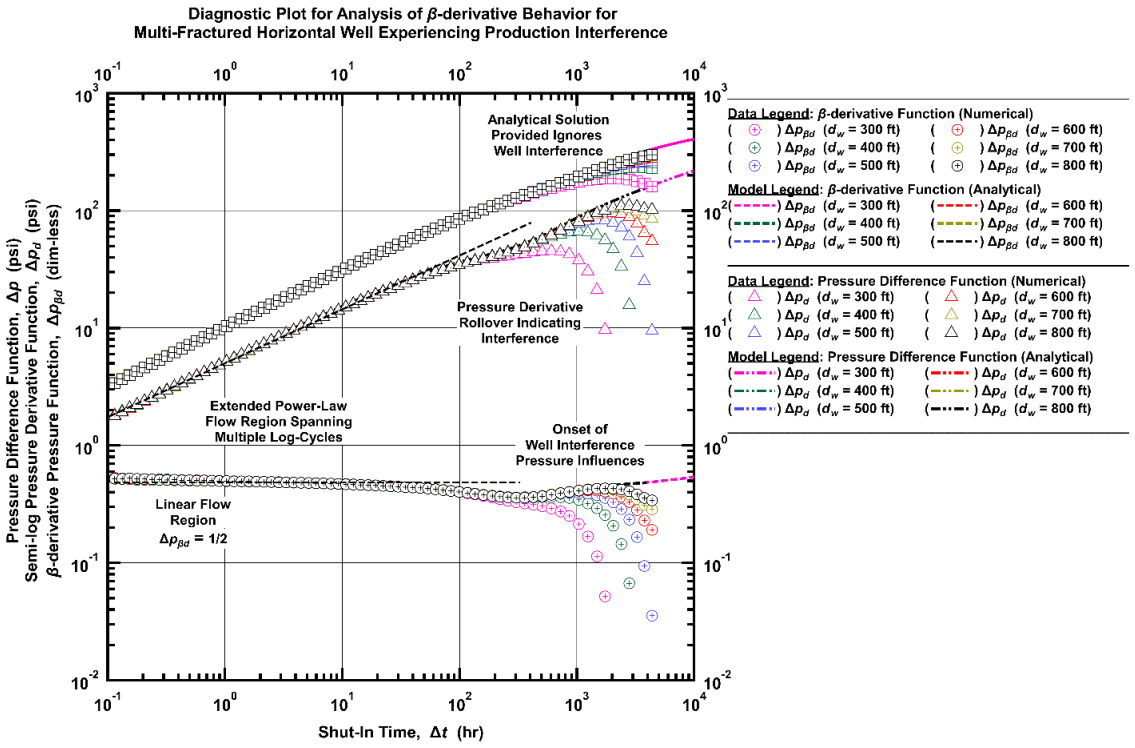

Figure 4.5 — Log-log scale for the diagnostic plot summarizing the results of the six numerical model scenarios simulated in this analysis related to well spacing for a shut-in prior-producing parent well as its offset child well is put-on-production. The well test derivative ("Bourdet" derivative) and the β-derivative are included to illustrate the characteristics these functions have as interference effects begin to be observed.

As all of the numerical model scenarios have the same hydraulic fracture spacing (*i.e.*, 250 feet), we do not observe appreciable fracture interference features in the diagnostic plot. In addition, since the only parameter being varied is the distance between parent and child wells (*i.e.*, the well spacing), only late-time behavior is different when the pressure front from the producing child well begins to reach the shut-in prior-producing parent well. This pressure influence is (obviously) more significant for closer-spaced well scenarios.

As an example, the 300-foot well spacing scenario begins to experience interference effects beginning at 350 hours of shut-in time. In contrast, the 800-foot well spacing scenario does not observe pressure interference until approximately 3000 hours. Finally, we can confirm that our interpretation of pressure interference from the β-derivative is consistent with what is actually observed by comparing the single-well analytical solution to the numerical results. Using the 800-foot well spacing scenario as example, we do note that the numerical and analytical results align until 3000 hours.

Desuperposition Analysis

In addition to interpreting the diagnostic plot for the pressure buildup profile, we also perform a "desuperposition" analysis. For this, we follow the methodology as described in Chu *et al*. [2020]. Put simply, we utilize the first 48-hours of stabilized pressure buildup data (before the child well is put on production) and fit a power-law trendline through the data. Using this regressed power-law function as a basis pressure function that is assumed to not contain pressure interference effects, we then take the pressure difference between the two-well numerical model and the regressed power-law function.

This yields a new pressure difference function that will serve as the basis for our "desuperposition" analysis. With this function, we also can compute the "Bourdet" well test derivative and the β-derivative for guidance in our analysis. **Figure 4.6** presents this desuperposition pressure function and the auxiliary pressure derivative functions on a log-log scale for the 800-foot well spacing scenario.

Using the β-derivative function, we note that a stabilized value approximately equal to 1.02 is reached at mid-time during the recorded pressure buildup. This region of stabilized β-derivative extends from 30 hours to 150 hours. Review of the pressure distribution profile at 150 hours, as generated by the numerical model, shows that the pressure front from the child well has not yet reached the parent well. Beyond 150 hours of shut-in time, however, a transition flow region occurs and is identified by the changing β-derivative function at this time. This behavior continues until a new β-derivative value equal to 0.71 is reached at approximately 1000 hours of shut-in time. Consulting the pressure distribution profile at this time, we note that significant pressure depletion has occurred between the hydraulic fractures of the child well as the pressure front has now propagated beyond the fracture tips and is beginning to influence the parent well.

From this interference analysis using the desuperposition method, we note a 30% change in β-derivative value as interference effects present themselves for the 800-foot well spacing scenario.

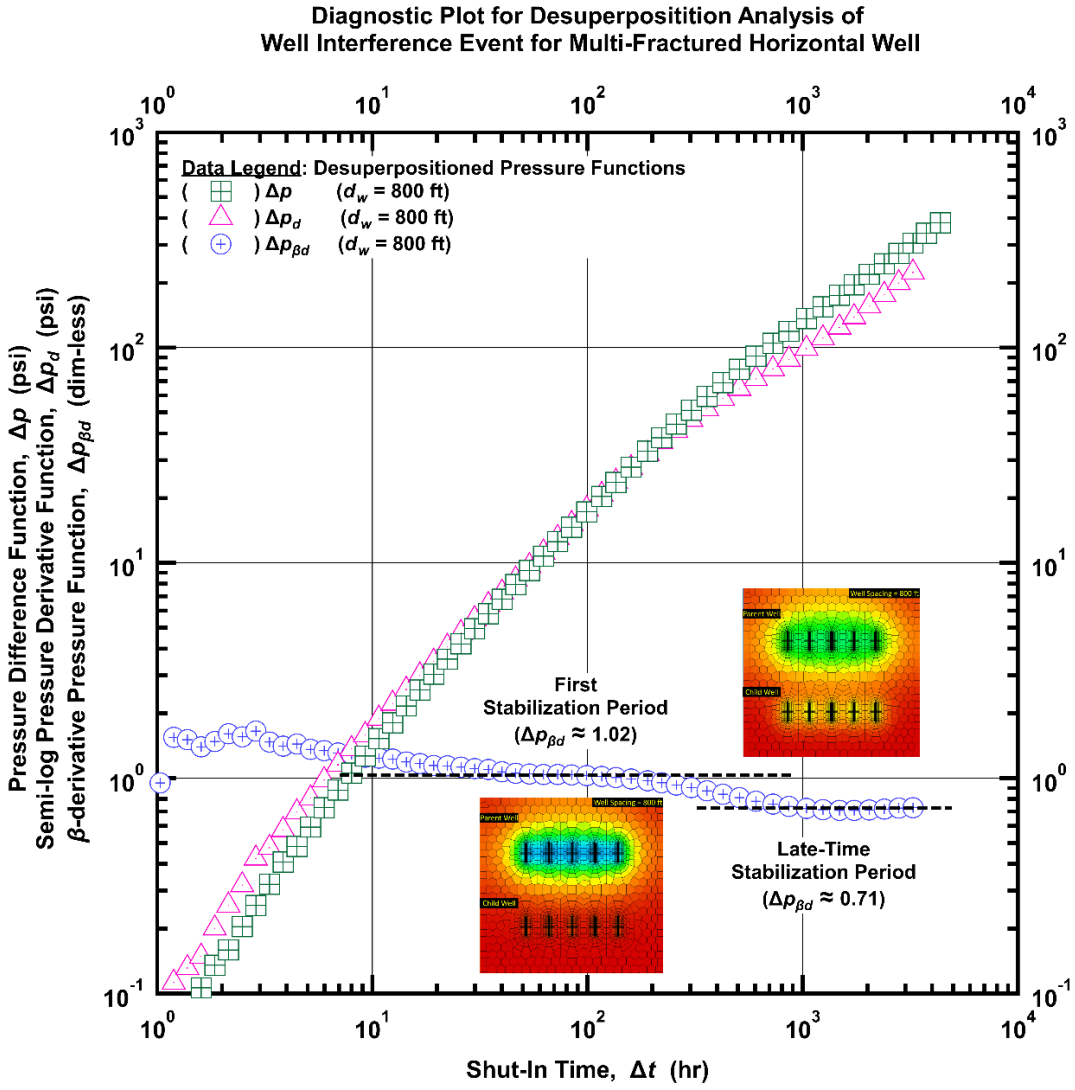

Figure 4.6 — Log-log scale diagnostic plot illustrate the "desuperposition" data associated with the 800-foot well spacing scenario for analyzing production interference between a recently put-on-production child well and a shut-in prior-producing parent well. The parent well (top) and child well (bottom) pressure profiles are embedded in this figure for selected shut-in times to illustrate the pressure distribution state in the model.

Pressure Distribution Evolution Based on Well Spacing

As a final approach to analyzing well spacing effects on pressure interference, we focus on the pressure distribution evolution at specified shut-in times. More specifically, when comparing the grid block pressure distributions at a given shut-in time, we observe what degree of interaction (or, "communication") has been detected by the shut-in prior-producing parent well. **Figure 4.7** presents an illustration of this analysis by comparing the well interference evolution observed between the 300-foot and 800-foot well spacing scenarios.

Comparing the pressure distribution profiles qualitatively, we note that the 300-foot well spacing scenario exhibits parent well depletion (due to its time on production) that very early on communicates with the pressure front caused by the child well being put on production. For the 800-foot well spacing scenario, the depletion from the parent well is also significant and extends beyond the hydraulic fracture tips, but significant distance between the parent and child well exist such that no interaction (or, "communication") is detected at a shut-in time of 40 hours. As early as 640 hours of shut-in time depletion of the reservoir between the two wells is observed for the 800-foot case and after 1040 hours is when a clear pressure interference characteristic is observable for the widest well spacing case. In contrast, the 300-foot well spacing scenario demonstrates significant well interference characteristics at 340 hours of shut-in time and by 1040 hours the two wells appear to be in near-complete communication and begin producing as a "total" system.

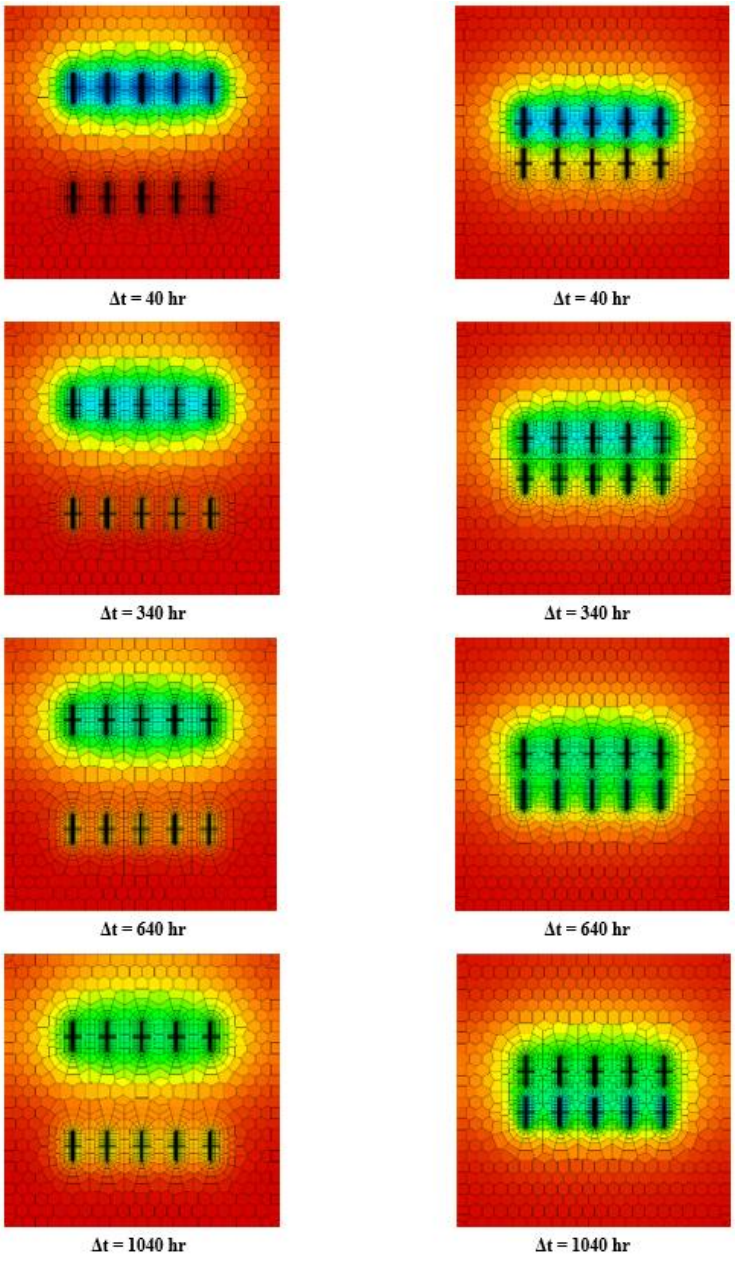

Figure 4.7 — Summary view of pressure distribution evolution in the reservoir and well models for the 800-ft (left) and 300-ft (right) well spacing scenarios. Both well spacing cases model a 1000-ft horizontal well with widely-spaced hydraulic fractures (250-ft spacing) evenly distributed across the lateral. Note that for each visual, the top well is the shut-in prior-producing parent well and the bottom well is the recently put-on-production child well.

CHAPTER V

SUMMARY, CONCLUSIONS, AND RECOMMENDATIONS

5.1. Summary

In this work we demonstrated the use of the trilinear flow model as a practical approach for analyzing the pressure behavior of a multi-fracture horizontal well (MFHW) in unconventional shale reservoirs. Through the use of type curves, we highlighted the influence of various phases of reservoir performance including: (a) flow within hydraulic fractures, (b) flow between hydraulic fractures, and (c) flow beyond hydraulic fractures. For each of these scenarios, we implemented the β-derivative pressure function as a means for identifying flow regimes and for interpreting characteristic parameters related to the reservoir and well systems, such as hydraulic fracture conductivity and transient dual porosity model parameters.

In addition, we provided two synthetic examples of interference events to represent scenarios that could be encountered in practice. We incorporated the β-derivative pressure into our analyses as a means of detecting the onset of pressure interference as it related to both hydraulic fracture spacing design and well spacing design. In addition to showing the utility of the β-derivative pressure function in identifying pressure interference, we highlighted the fundamental relation that the β-derivative function has to the power-law exponent, which is influential in characterizing flow regimes commonly encountered in multi-fracture horizontal wells (*e.g.*, linear flow).

5.2. Conclusions

As a result of this work the following conclusions are derived:

- Unconventional shale reservoirs exhibit complex, transient flow behavior due to the interaction of hydraulic fractures with the reservoir and the heterogeneities that are present at all scales.
- Pressure-transient testing is still relevant for unconventional shale assets and can be practically implemented by operators.
- The trilinear flow model, as developed by Brown et al. [2011], serves as a practical reservoir model for the diagnostic pressure-transient analysis of multi-fracture horizontal wells.
- Meaningful PTA work requires holistic treatment of available data in order to yield unique insights and diagnostics (*e.g.*, completion reports, accurate PVT data, etc.).
- The β-derivative provides unique characteristics related to power-law flow regimes when incorporated as a plotting function. Direct interpretation of the β-derivative to yield the power-law exponent is a clear advantage of this function and it can be readily applied to any analysis (PTA or RTA).
- Incorporation of the β-derivative pressure function in pressure-transient analysis can be useful in "repurposing" conventional methods of analysis to aid in addressing modern industry challenges related to well spacing design and level of "connectivity" observed in the field.

5.3. Recommendations for Future Work

We recommend the following for future research:

- Applying the trilinear flow model to general variable-rate/variable-pressure drop cases using superposition.
- Continuing the development of analytical solutions that model multiple multi-fracture horizontal wells in a reservoir with natural fractures connecting flow between the wells.
- Incorporating fractal theory in the study of heterogeneity effects in unconventional shale reservoirs. Additionally, further development related to explaining the fractal theory model parameters relationship to physical reservoir properties is key for possible adoption by engineers.

NOMENCLATURE

General Variables:

C_{Df} = Dimensionless wellbore storage coefficient

C_f = Formation compressibility, $psia^{-1}$

C_{fD} = Dimensionless hydraulic fracture conductivity

C_s = Wellbore storage constant, bbl/psi

d_f = Hydraulic fracture spacing, ft

d_w = Well spacing, ft

F_c = Hydraulic fracture conductivity, md-ft

h = Net pay thickness, ft

h_m = Matrix slab thickness, ft

h_{nf} = Natural fracture thickness, ft

k = Permeability, md

L_w = Horizontal well length, ft

n_f = Number of hydraulic fractures

n_{grid} = Number of grid blocks in simulation case

Δn_{grid} = Change in number of grid blocks relative to base case, percent

p = Bottomhole pressure, psia

p_i = Initial reservoir pressure, psia

Δp = Pressure drop (pressure buildup case), psi

$\Delta p_{\beta d}$ = β-derivative (pressure), dimensionless

Δp_d = Well testing pressure derivative ("Bourdet" derivative), psi

p_D = Dimensionless pressure

p_{Di} = Dimensionless pressure integral

p_{pd} = Primary pressure derivative ("Cartesian" derivative), psi/hr

q = Flowrate, STB/D

r_w = Wellbore radius, ft

R^2 = Coefficient of determination

s = Skin factor, dimensionless

S = Fluid saturation, fraction

t = Time, hr

T_r = Reservoir Temperature, °F

Δt = Shut-in time, hr

t_p = Producing time, hr

w_f = Hydraulic fracture width, ft

w_{fD} = Dimensionless hydraulic fracture width

x_f = Hydraulic fracture half-length, ft

Greek Symbols:

α = Grouping parameter, dimensionless

γ = Specific gravity, fraction

λ = Interporosity flow coefficient ("Flow-capacity" ratio), dimensionless

ϕ = Porosity, fraction

ω = Storativity ratio, dimensionless

Subscripts:

o = oil

g = gas

w = water

Acronyms:

BHP = Bottomhole pressure

CPG = Chow pressure group

DFIT = Diagnostic fracture-injection/falloff test

DFN = Discrete fracture network

DOD = Depth of Detection

EUR = Estimated ultimate recovery

FBA = Flowback Analysis

FDI = Fracture driven interaction

LWD = Logging While Drilling

MFHW = Multi-fracture horizontal well

MWD = Measure While Drilling

ODE = Ordinary differential equation

PBU = Pressure buildup

PDD = Pressure drawdown

PDE = Partial differential equation

PTA = Pressure-transient analysis

ROI = Radius of Investigation

RTA = Rate-transient analysis

SRV = Stimulated reservoir volume

US-EIA = United States Energy Information Administration

REFERENCES

Ballinger, B., Green, B., Vajjha, P., et al. (2022) "Understanding the Hydraulic and Conductive Half Lengths in the Bakken/Three Forks Play – Coupling Sealed Wellbore Pressure Monitoring SWPM and Chow Pressure Group CPG." Paper SPE-209144-MS presented at the SPE Hydraulic Fracturing Technology Conference and Exhibition, The Woodlands, Texas, USA, February 2022. doi: https://doi.org/10.2118/209144-MS

Barree, R.D., Fisher, M.K., and Woodroof, R.A., (2002) "A Practical Guide to Hydraulic Fracture Diagnostic Technologies." Paper SPE-77442-MS presented at the SPE Annual Technical Conference and Exhibition, San Antonio, Texas, USA, 29 September-2 October 2002. doi: https://doi.org/10.2118/77442-MS

Blasingame, T.A., Johnston, J.L., and Lee, W.J. (1989) "Type-Curve Analysis Using the Pressure Integral Method." Paper SPE-18799-MS presented at the SPE California Regional Meeting, Bakersfield, California, USA, April 1989. doi: https://doi.org/10.2118/18799-MS

Bourdet, D., Ayoub, J.A., and Pirard, Y.M. (1989) "Use of Pressure Derivative in Well-Test Interpretation." *SPEFE* 4, 293–302. doi: https://doi.org/10.2118/12777-PA

Britt, L.K., Jones, J.R., and Miller II, W.K. (2010) "Defining Horizontal Well Objectives in Tight and Unconventional Gas Reservoirs." Paper SPE-137839-MS presented at the Canadian Unconventional Resources & International Petroleum Conference, Calgary, Alberta, Canada, October 2010. doi: https://doi.org/10.2118/137839-MS

Brown, M., Ozkan, E., Raghavan, R., et al. (2011) "Practical Solutions for Pressure-Transient Responses of Fractured Horizontal Wells in Unconventional Shale Reservoirs." *SPEREE* 14: 663–676. doi: https://doi.org/10.2118/125043-PA

Bryan, E.W., Symmons, D., Ilk, D., et al. (2021) "The Utilization of the "Rate-Integral" to Assist with Decline Curve Analysis of Poor-Quality Unconventional Time-Rate Data." Paper URTeC-2021-5519 presented at the SPE/AAPG/SEG Unconventional Resources Technology Conference, Houston, Texas, USA, July 2021. doi: https://doi.org/10.15530/urtec-2021-5519

Chapa, S. (2019) "Drilling Down: The 10 Longest Horizontal Wells in Texas." *Chron*. url: https://www.chron.com/business/energy/article/Drilling-Down-The-10-longest-horizontal-wells-in-14908451.php. Accessed 25 May 2022.

Chen, C.C., and Raghavan, R. (1997) "A Multiply-Fractured Horizontal Well in a Rectangular Drainage Region." *SPEJ* 2, 455–465. doi: https://doi.org/10.2118/37072-PA

Chow, V.T. (1952) "On the Determination of Transmissibility and Storage Coefficients from Pumping Test Data." *Trans. Am. Geophys. Un.* 33, 397–404.

Chu, W.C., Pandya, N., Flumerfelt, R.W., et al. (2017) "Rate-Transient Analysis Based on Power-Law Behavior for Permian Wells." Paper SPE-187180-MS presented at the SPE Annual Technical Conference and Exhibition, San Antonio, Texas, USA, October 2017. doi: https://doi.org/10.2118/187180-MS

Chu, W.C., Scott, K.D., Flumerfelt, R., et al. (2020) "A New Technique for Quantifying Pressure Interference in Fractured Horizontal Shale Wells." *SPEREE* 23: 143–157. doi: https://doi.org/10.2118/191407-PA

Cinco-L., H., Samaniego-V., F., and Dominguez-A., N. (1978) "Transient Pressure Behavior for a Well With a Finite-Conductivity Vertical Fracture." Paper SPE-6014-PA presented at the SPE-AIME 51st Annual Fall Technical Conference and Exhibition, New Orleans, Louisiana, 3-6 October 1976. doi: https://doi.org/10.2118/6014-PA

Cinco-L., H., and Samaniego-V., F. (1981) "Transient Pressure Analysis: Finite Conductivity Fracture Case Versus Damaged Fracture Case." Paper SPE-10179-MS presented at the SPE-AIME 56th Annual Fall Technical Conference and Exhibition, San Antonio, Texas, 5-7 October 1981. doi: https://doi.org/10.2118/10179-MS

Cinco-L., H., and Samaniego-V., F. (1981) "Transient Pressure Analysis for Fractured Wells." *JPT* 33 (1981): 1749–1766. doi: https://doi.org/10.2118/7490-PA

Cinco-L., H. (1982) "Evaluation of Hydraulic Fracturing By Transient Pressure Analysis Methods." Paper SPE-10043-MS presented at the SPE International Petroleum Exhibition and Technical Symposium, Beijing, China, 18-26 March 1982. doi: https://doi.org/10.2118/10043-MS

Cipolla, C.L. and Wright, C.A. (2000) "Diagnostic Techniques to Understand Hydraulic Fracturing: What? Why? And How?" Paper SPE-59735-MS presented at the SPE/CERI Gas Technology Symposium, Calgary, Alberta, Canada, 3-5 April 2000. doi: https://doi.org/10.2118/59735-MS

Cipolla, C., Mack, M., and Maxwell, S. (2010) "Reducing Exploration and Appraisal Risk in Low Permeability Reservoirs Using Microseismic Fracture Mapping—Part 2." Paper SPE-138103-MS presented at the SPE Latin American & Caribbean Petroleum Eng. Conf., Lima, Peru, 1-3 December 2010. doi: https://doi.org/10.2118/138103-MS

Craig, D.P. (2017) "Determining Fracture Geometry in a Multifractured Horizontal Well Using DFIT Interpretation, Intra-well Fracture-To-Fracture Interference, and Production History Matching." Paper URTeC-2695331-MS presented at the Unconventional Resources Technology Conference, Austin, Texas, USA, 24-26 July 2017. doi: https://doi.org/10.15530/urtec-2017-2695331

Cruz, F., Tinni, A., Brackeen, S., Sondergeld, C. et al. (2020) "Impact of Capillary Pressure on Total Porosity in Unconventional Shales." Paper URTeC-2020-3117

presented at the SPEE/AAPG/SEG Unconventional Resources Technology Conference, Virtual, 20-22 July. doi: https://doi.org/10.15530/urtec-2020-3117

Escobar, F.H., Navarrete, J.M., and Losada, H.D. (2004) "Evaluation of Pressure Derivative Algorithms for Well-Test Analysis." Paper SPE-86936-MS presented at the SPE International Thermal Operations and Heavy Oil Symposium and Western Regional Meeting, Bakersfield, California, USA, March 2004. doi: https://doi.org/10.2118/86936-MS

Flamenco-Lopez, F., and Camacho-Velazquez, R. (2003) "Determination of Fractal Parameters of Fracture Networks Using Pressure-Transient Data." *SPEREE* 6: 39–47. doi: https://doi.org/10.2118/82607-PA

Fulford, D.S., and Blasingame, T.A. (2020) "Optimization Methods for Time-Rate-Pressure Production Data Analysis using Automatic Outlier Filtering and Bayesian Derivative Calculations." Paper SPE-201404-MS presented at the SPE Annual Technical Conference and Exhibition, Virtual, October 2020. doi: https://doi.org/10.2118/201404-MS

Gringarten, A.C., and Ramey, H.J., (1973) "The Use of Source and Green's Functions in Solving Unsteady-Flow Problems in Reservoirs." *SPEJ* 13: 285–296. doi: https://doi.org/10.2118/3818-PA

Gringarten, A.C., and Ramey, H.J., (1974) "Unsteady-State Pressure Distributions Created by a Well With a Single Horizontal Fracture, Partial Penetration, or Restricted Entry." *SPEJ* 14 (04): 413–426. doi: https://doi.org/10.2118/3819-PA

Gringarten, A.C., Ramey, H.J., and Raghavan, R., (1974) "Unsteady-State Pressure Distributions Created by a Well With a Single Infinite-Conductivity Vertical Fracture." *SPEJ* 14 (04): 347–360. doi: https://doi.org/10.2118/4051-PA

Gringarten, A.C., and Ramey, H.J., (1975) "An Approximate Infinite Conductivity Solution for a Partially Penetrating Line-Source Well." *SPEJ* 15 (02): 140–148. doi: https://doi.org/10.2118/4733-PA

Haghshenas, B., and Qanbari, F., (2021) "Pressure Depletion Mapping Using Multi-Well DFITs and its Applications in Hydraulic Fracture Characterization and Permeability Estimation: Examples from Montney Formation." Paper SPE-204191-MS presented at the SPE Hydraulic Fracturing Technology Conference and Exhibition, Virtual, 4-6 May 2021. doi: https://doi.org/10.2118/204191-MS

Hantush, M.S., (1957) "Nonsteady Flow to a Well Partially penetrating an Infinite Leaky Aquifer." *Proceedings.* Iraq Scientific Society.

Haustveit, K., Dahlgren, K., Greenwood, H., et al (2017) "New Age Fracture Mapping Diagnostic Tools — A STACK Case Study." Paper SPE-184862-MS presented at the SPE Hydraulic Fracturing Technology Conference and Exhibition, The Woodlands, Texas, USA, 24-26 January 2017. doi: https://doi.org/10.2118/184862-MS

Heintzelman, L., Willerth, M., Elhaj, N., et al (2022) "Field Validation of an Automated Geosteering Algorithm in the Haynesville Shale." Paper SPE-208697-MS presented at the IADC/SPE International Drilling Conference and Exhibition, Galveston, Texas, USA, 8-10 March 2022. doi: https://doi.org/10.2118/208697-MS

Holditch, S.A. (2006) "Tight Gas Sands." (invited article) *JPT* 58 (6): 86-93. doi: https://doi.org/10.2118/103356-JPT

Hosseinpour-Zonoozi, N., Ilk, D., and Blasingame, T.A. (2006) "The Pressure Derivative Revisited–Improved Formulations and Applications." Paper SPE-103204-MS presented at the SPE Annual Technical Conference and Exhibition, San Antonio, Texas, USA, September 2006. doi: https://doi.org/10.2118/103204-MS

Ilk, D. (2010) "Well Performance Analysis for Low to Ultra-Low Permeability Reservoir Systems." Doctoral dissertation, Texas A&M University, College Station, Texas, USA. Available electronically from https://hdl.handle.net/1969.1/ETD-TAMU-2010-08-8574

Kamal, M. and Brigham, W.E. (1975) "The Effect of Linear Pressure Trends on Interference Tests." *JPT* 27 (11): 1383–1384. doi: https://doi.org/10.2118/4967-PA

Kuuskraa, V.A., Oudinot, A., and Koperna, G.J. (2019) "Reservoir Simulation of Enhanced Oil Recovery: Wolfcamp Shale/Midland Basin." National Energy Technology Laboratory (2019).

Lane, H.S., Lee, W.J., and Watson, A.T. (1991) "An Algorithm for Determining Smooth, Continuous Pressure Derivatives From Well-Test Data." *SPEFE* 6, 493–499. doi: https://doi.org/10.2118/20112-PA

Larsen, L., and Hegre, T.M. (1991) "Pressure-Transient Behavior of Horizontal Wells With Finite Conductivity Vertical Fractures." Int. Artic Tech. Conf. Anchorage, Alaska, USA, 29-31 May. SPE-22076-MS. doi: https://doi.10.2118/22076-MS

Lee, W.J., Rollins, J.B., and Spivey, J.P. (2003) "Pressure Transient Testing." *Society of Petroleum Engineers*. Texas, United States.

Lerza, A., Cuervo, S., and Malhotra, S. (2021) "Closing the Gap in Characterizing the Parent Child Effect for Unconventional Reservoirs — A Case of Study in Vaca Muerta Shale Formation." Paper SPE-206001-MS presented at the SPE Annual Technical Conf. and Exhibition, Dubai, UAE, 21-23 Sep 2021. doi: https://doi.10.2118/206001-MS

Martin, A.N. and Rylance, M. (2010) "Hydraulic Fracturing Makes the Difference: New Life for Old Fields." Paper SPE-127743-MS presented at the North Africa Technical Conference and Exhibition, Cairo, Egypt, 14-17 February 2010.

Masters, J.A. (1979) "Deep Basin Gas Trap, Western Canada" *AAPG Bulletin* 63 (2): 152–181. doi: https://doi.org/10.1306/C1EA55CB-16C9-11D7-8645000102C1865D

Mattar, L., and Zaoral, K. (1992) "The Primary Pressure Derivative (PPD) – A New Diagnostic Tool In Well Test Interpretation." *JCPT* 31. doi: https://doi.org/10.2118/92-04-06

Mayerhofer, M.J., Richardson, M.F., Walker Jr., R.N., et al (1997) "Proppants? We Don't Need No Proppants." Paper SPE-38611-MS presented at the SPE Annual Technical Conference and Exhibition, San Antonio, Texas, USA, 05-08 October 1997. doi: https://doi.org/10.2118/38611-MS

Mayerhofer, M.J., Bolander, J.L., Williams, L.I., et al (2005) "Integration of Microseismic Fracture Mapping, Fracture and Production Analysis With Well Interference Data To Optimize Fracture Treatments in the Overton Field, East Texas." Paper SPE-95508-MS presented at the SPE Annual Technical Conference and Exhibition, Dallas, Texas, USA, 9-12 October 2005. doi: https://doi.org/10.2118/95508-MS

Mayerhofer, M.J., Lolon, E.P., Youngblood, J.E., et al (2006) "Integration of Microseismic Fracture Mapping Results With Numerical Fracture Network Production Modeling in the Barnett Shale." Paper SPE-102103-MS presented at the SPE Annual Technical Conference and Exhibition, San Antonio, Texas, USA, 24-27 September 2006. doi: https://doi.org/10.2118/102103-MS

McNeil, F., van Gijtenbeek, K., and van Domelen, M. (2012) "New Hydraulic Fracturing Process Enables Far-Field Diversion in Unconventional Reservoirs." Paper SPE-152704-MS presented at the SPE/EAGE European Unconventional Resources Conference and Exhibition, Vienna, Austria, 20-22 March 2012. doi: https://doi.org/10.2118/152704-MS

Medeiros, F., Ozkan, E., and Kazemi, H. (2008) "Productivity and Drainage Area of Fractured Horizontal Wells in Tight Gas Reservoirs." *SPE Res Eval & Eng* 11 (2008): 902—911. doi: https://doi.org/10.2118/108110-PA

Mottahedeh, R. (2008) "Horizontal Well Geosteering: Planning, Monitoring and Geosteering." *J Can Pet Technol* 47 (2008): 28–32. doi: https://doi.org/10.2118/08-11-28-CS

Muskat, M. (1946) "The Flow of Homogeneous Fluids Through Porous Media." *McGraw-Hill*. New York, United States.

Nicholson, A.K., Hawkes, R.B., and Bachman, R.C., (2019) "Early Warning Systems — Using PTA Analysis of DFITs to Understand Complex Hydraulic Fractures and Optimize Treatment Designs." Paper SPE-196194-MS presented at the SPE Annual Technical Conference and Exhibition, Calgary, Alberta, Canada, 30 September – 2 October 2019. doi: https://doi.org/10.2118/196194-MS

Onur, M., Peres, A.M.M., and Reynolds, A.C. (1989) "New Pressure Functions for Well Test Analysis." Paper SPE-19819-MS presented at the SPE Annual Technical Conference and Exhibition, San Antonio, Texas, USA, October 1989. doi: https://doi.org/10.2118/19819-MS

Ozkan, E., and Raghavan, R. (1991) "Some New Solutions to Solve Problems in Well Test Analysis: I — Computational Considerations and Applications." *SPE Form Eval* 6 (1991): 369-378. doi: https://doi.org/10.2118/18616-PA

Palisch, T.T., Vincent, M.C., and Handren, P.J. (2008) "Slickwater Fracturing — Food for Thought." Paper SPE-115766-MS presented at the SPE Annual Technical Conference and Exhibition, Denver, Colorado, USA, 21-24 September 2008. doi: https://doi.org/10.2118/115766-MS

Pathi, V.S., Kurison, C., Hakami, A.M. et al. (2022) "Limited Storage and Recovery of Adsorbed Gas in Shale Reservoirs — Insights From Experiments and Production Modeling." *Fuel Com.* 10 (1000339). doi: https://doi.org/10.1016/j.jfueco.2021.100039

Poe, B.D. (2014) "Production Performance Evaluation of Wells Completed in Unconventional Reservoirs Using Capillary Pressure Data and Relative Permeability Effects." Paper SPE-170940-MS presented at the SPE Annual Technical Conference and Exhibition, Amsterdam, 27-29 October. doi: https://doi.org/10.2118/170940-MS

Raghavan, R. (1980) "The Effect of Producing Time on Type Curve Analysis." *JPT* 32 (6): 1053–1064. SPE-6997-PA. doi: https://doi.org/10.2118/6997-PA

Rahman, K. and Gui, F. (2016) "Geomechanical Sweet Spot Identification in Unconventional Resources Development." Paper SPE-182247-MS presented at the SPE Asia Pacific Oil & Gas Conference and Exhibition, Perth, Australia, 25-27 October 2016. doi: https://doi.org/10.2118/182247-MS

Rushing, J.A. and Sullivan, R.B. (2003) "Evaluation of a Hybrid Waterfrac Stimulation Technology in the Bossier Tight Gas Sand Play." Paper SPE-84394-MS presented at the SPE Annual Technical Conference and Exhibition, Denver, Colorado, USA, 05-08 October 2003. doi: https://doi.org/10.2118/84394-MS

Rushing, J.A., Sullivan, R.B., and Blasingame, T.A., (2005) "Post-Fracture Performance Diagnostics for Gas Wells With Finite-Conductivity Vertical Fractures." Paper SPE-97972-MS presented at the SPE Eastern Regional Meeting, Morgantown, West Virginia, USA, 14-16 September 2005. doi: https://doi.org/10.2118/97972-MS

Saint, C., Martakov, S., Mumtaz, A., et al (2014) "Case Study: Application of Azimuthal Resistivity, Azimuthal Density, and Resistivity Inversion to Geosteer in a Clastic Stringer, Saudi Arabia." Paper SPE-172181-MS presented at the SPE Saudi Arabia Section Annual Technical Symposium and Exhibition, Al-Khobar, Saudi Arabia, 21-24 April 2014. doi: https://doi.org/10.2118/172181-MS

Santoso, G., Denichou, J., Al-Alqum, W., et al (2022) "Collaborative Web Based Platform for 3D Reservoir Characterization and Geosteering Planning on the Cloud." Paper IPTC-22203-EA presented at the International Petroleum Technology Conference, Riyadh, Saudi Arabia, 21-23 February 2022. doi: https://doi.org/10.2523/IPTC-22203-EA

Serra, K., Reynolds, A.C., and Raghavan, R. (1983) "New Pressure Transient Analysis Methods for Naturally Fractured Reservoirs." *JPT* 2271–2283. doi: https://doi.org/10.2118/10780-PA

Somanchi, K., Brewer, J., and Reynolds, A., (2017) "Extreme Limited Entry Design Improves Distribution Efficiency in Plug-n-Perf Completions: Insights from Fiber-Optic Diagnostics." Paper SPE-184834-MS presented at the SPE Hydraulic Fracturing Technology Conference and Exhibition, The Woodlands, Texas, USA, 24-26 January 2017. doi: https://doi.org/10.2118/184834-MS

Sondergeld, C.H., Newsham, K.E., Comisky, J.T. et al. (2010) "Petrophysical Considerations in Evaluating and Producing Shale Gas Resources." Paper SPE-131768-MS presented at the SPE Unconventional Gas Conference, Pittsburgh, Pennsylvania, USA, 23-25 February. doi: https://doi.org/10.2118/131768-MS

Sowers, S. (2005) "The Bourdet Derivative Algorithm Revisited — Introduction and Validation of the Power-Law Derivative Algorithm for Applications in Well-Test Analysis." (internal) B.S. Report, Texas A&M University, College Station, Texas, USA

Timonov, A., Khabibullin, R.A., Gurbatov, N.S., et al (2021) "Automated Geosteering Optimization Using Machine Learning." Paper SPE-207364-MS presented at the Abu Dhabi International Petroleum Exhibition & Conference, Abu Dhabi, UAE, 15-18 November 2021. doi: https://doi.org/10.2118/207364-MS

Ugueto-C., G.A., Huckabee, P.T., Molenaar, M.M., et al (2016) "Perforation Cluster Efficiency of Cemented Plug and Perf Limited Entry Completions; Insights From Fiber Optics Diagnostics." Paper SPE-179124-MS presented at the SPE Hydraulic Fracturing Technology Conference, The Woodlands, Texas, USA, 9-11 February 2016. doi: https://doi.org/10.2118/179124-MS

U.S. Energy Information Administration (2011) "The Geology of Natural Gas Resources." *Today in Energy*.
url:https://www.eia.gov/todayinenergy/detail.php?id=110. Accessed 13 May 2022

U.S. Energy Information Administration (2019) "Horizontally Drilled Wells Dominate U.S. Tight Formation Production," *Today in Energy.*
url: https://www.eia.gov/todayinenergy/detail.php?id=39752. Accessed 25 May 2022

U.S. Energy Information Administration (2022) "Crude Reserves and Production — Tight Oil Production Estimates by Play." *Petroleum & Other Liquids*.
url: https://www.eia.gov/petroleum/data.php. Accessed 01 June 2022

U.S. Energy Information Administration (2022) "Proved Reserves of Crude Oil and Natural gas in the United States, Year-End 2020." *Independent Statistics & Analysis*. url: https://www.eia.gov/naturalgas/crudeoilreserves/pdf/usreserves.pdf. Accessed 29 May 2022

van Everdingen, A.F., and Hurst, W., (1949) "The Application of the Laplace Transformation to Flow Problems in Reservoirs." *JPT* 1 (1949): 305–324: doi: https://doi.org/10.2118/949305-G

Walker, R.N. Jr., Hunter, J.L., Brake, A.C., et al (1998) "Proppants, We Still Don't Need No Proppants — A Perspective of Several Operators." Paper SPE-49106-MS presented at the SPE Annual Technical Conference and Exhibition, New Orleans, Louisiana, USA, 27-30 September 1998. doi: https://doi.org/10.2118/49106-MS

Wang, H., and Sharma, M., (2020) "A Rapid Injection Flow-Back Test RIFT to Estimate In-Situ Stress and Pore Pressure in a Single Test." Paper SPE-199732-MS presented at the SPE Hydraulic Fracturing Technology Conference and Exhibition, The Woodlands, Texas, USA, 4-6 February 2020. doi: https://doi.org/10.2118/199732-MS

Wheaton, B., Haustveit, K., Deeg, W., et al (2016) "A Case Study of Completion Effectiveness in the Eagle Ford Shale Using DAS/DTS Observations and Hydraulic Fracture Modeling." Paper SPE-179149-MS presented at the SPE Hydraulic Fracturing Technology Conference, The Woodlands, Texas, USA, 9-11 February 2016. doi: https://doi.org/10.2118/179149-MS

Wolhart, S.L., Odegard, C.E., Warpinski, N.R., et al (2005) "Microseismic Fracture Mapping Optimizes Development of Low-Permeability Sands of the Williams Fork Formation in the Piceance Basin." Paper SPE-95637-MS presented at the SPE Annual Technical Conference and Exhibition, Dallas, Texas, USA, 9-12 October 2005. doi: https://doi.org/10.2118/95637-MS

Woodward, R. and Noynaert, S. (2017) "If It's So Easy, Why Don't You Come Do It Yourself? A Response to "What I Wish My Geologist Knew About Drilling: A Drilling Engineer's View of Geosteering"." Paper URTeC-2697532-MS presented at the Unconventional Resources Technology Conference, Austin, Texas, USA, 24-26 July 2017. doi: https://doi.org/10.15530/URTEC-2017-2697532

Zanganeh, B., Clarkson, C.R., Cote, A., and Richards, B. (2020) "Field Trials of the New DFIT-Flowback Analysis (DFIT-FBA) for Accelerated Estimates of Closure and Reservoir Pressure and Reservoir Productivity." Paper URTeC-2838-MS presented at the Unconventional Resources Technology Conference, Austin, Texas, USA, 20-22 July 2020. doi: https://doi.org/10.15530/urtec-2020-2838

Zeinabady, D., Zanganeh, B., Shahamat, S., and Clarkson, C.R., (2021) "Application of DFIT-FBA Tests Performed at Multiple Points in a Horizontal Well for Advanced Treatment Stage Design and Reservoir Characterization." Paper SPE-204200-MS presented at SPE Hydraulic Fracturing Technology Conference and Exhibition, Virtual, 4-6 May 2021. doi: https://doi.org/10.2118/204200-MS

Zhao, G., Jin, B., Yang, L, et al (2022) "Next Level of Complex Reservoir Geosteering: The New Generation of Ultra-High-Definition Directional Resistivity Propagation Method." Paper IPTC-22208-EA presented at the International Petroleum Technology Conference, Riyadh, Saudi Arabia, 21-23 Feb 2022. doi: https://doi.org/10.2523/IPTC-22208-EA

APPENDIX A

ADDITIONAL TYPE CURVES GENERATED USING THE TRILINEAR FLOW MODEL

In this appendix we provide additional type curves generated for the case of a multi-fracture horizontal well in unconventional shale reservoir. The reservoir, well, and fluid descriptions as presented by Brown *et al*. [2011] are reflected in our base analysis to validate our programming of the pressure-transient solution. From there, we generate type curves that vary various well and reservoir parameters.

The following type curve cases are presented in this appendix:

1. Varying hydraulic fracture conductivity for a multi-fracture horizontal well (MFHW) within a homogeneous reservoir.
2. Varying hydraulic fracture conductivity for a multi-fracture horizontal well (MFHW) within a dual porosity reservoir with pseudosteady-state interporosity flow conditions.
3. Multi-fracture horizontal well (MFHW) with varying flow-capacity ratio and wellbore storage within a dual porosity reservoir with pseudosteady-state interporosity flow conditions.
4. Multi-fracture horizontal well (MFHW) with varying storativity ratio, varying flow-capacity ratio, and wellbore storage within a dual porosity reservoir with pseudosteady-state interporosity flow conditions.

A.1. Varying Hydraulic Fracture Conductivity For a Multi-Fracture Horizontal Well (MFHW) Within a Homogeneous Reservoir.

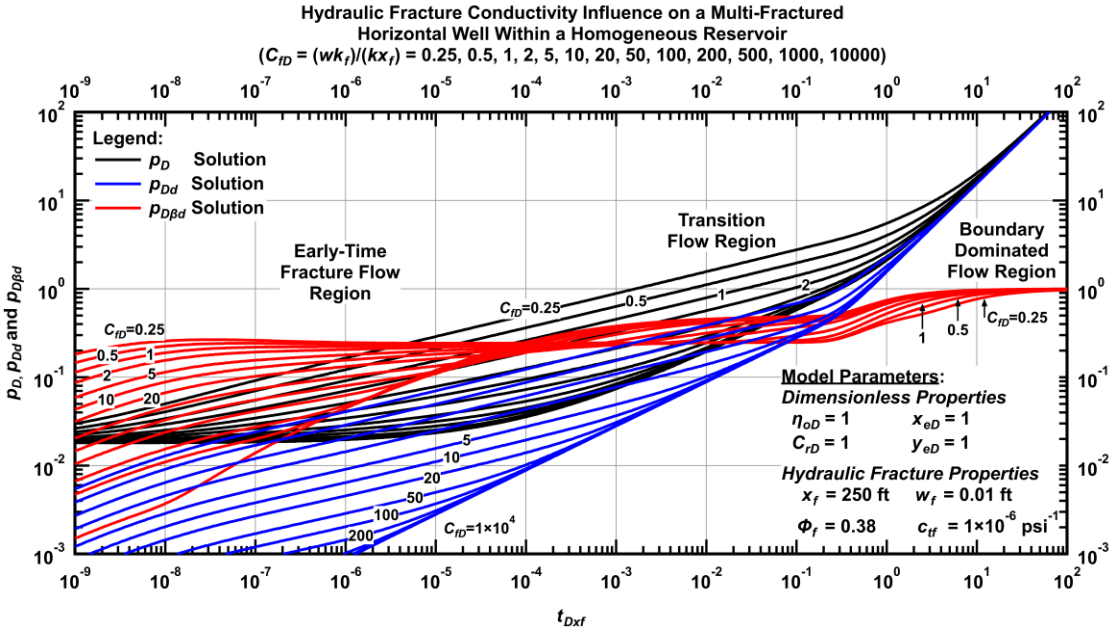

Figure A.1 — Log-log scale diagnostic plot for varying hydraulic fracture conductivity for a multi-fracture horizontal well with no wellbore storage effects within a homogeneous reservoir.

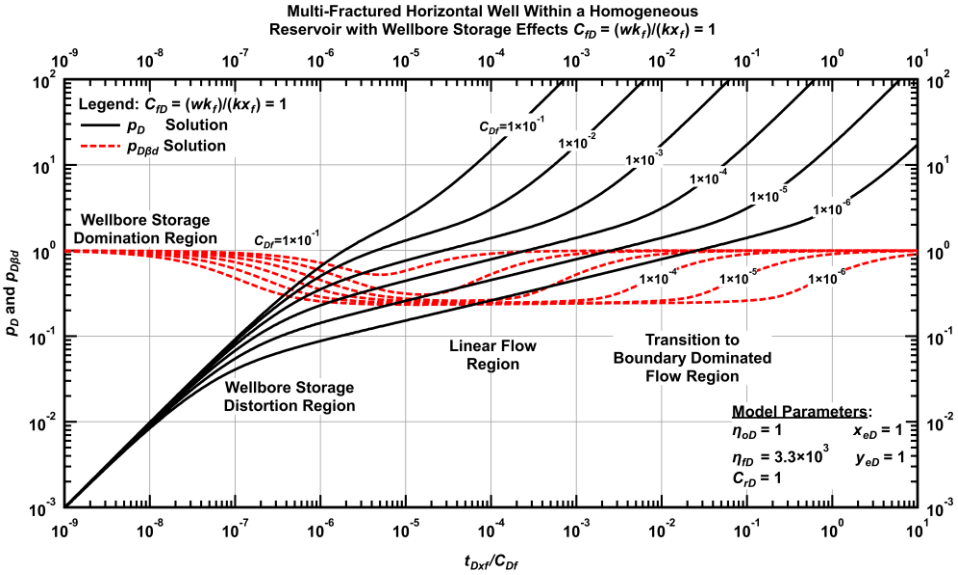

Figure A.2 — Log-log scale diagnostic plot for a multi-fracture horizontal well with varying wellbore storage effects within a homogeneous reservoir (C_{fD} = 1).

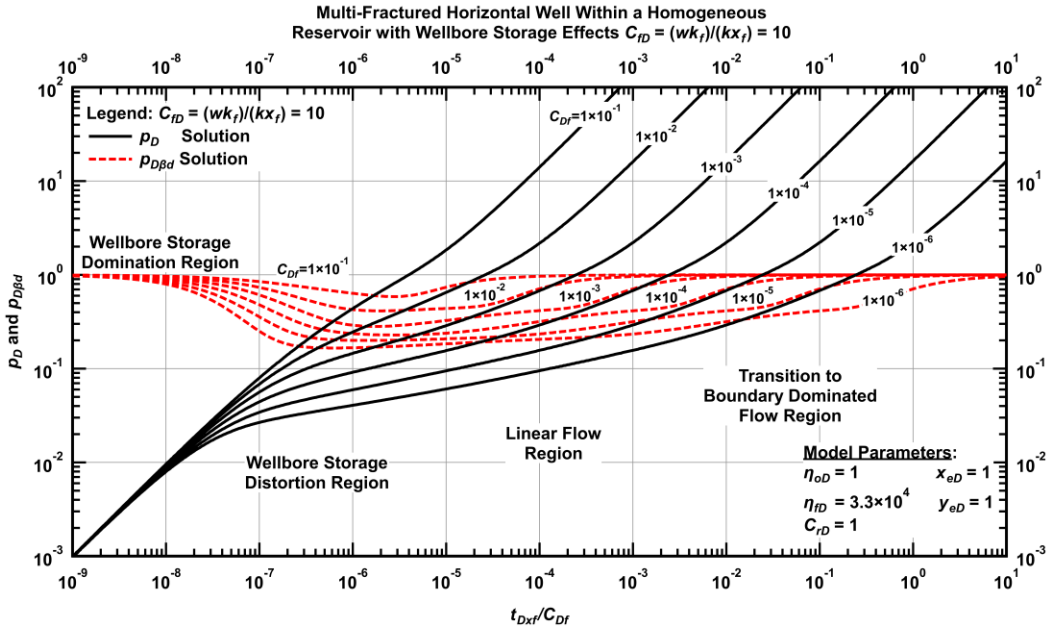

Figure A.3 — Log-log scale diagnostic plot for a multi-fracture horizontal well with varying wellbore storage effects within a homogeneous reservoir (C_{fD} = 10).

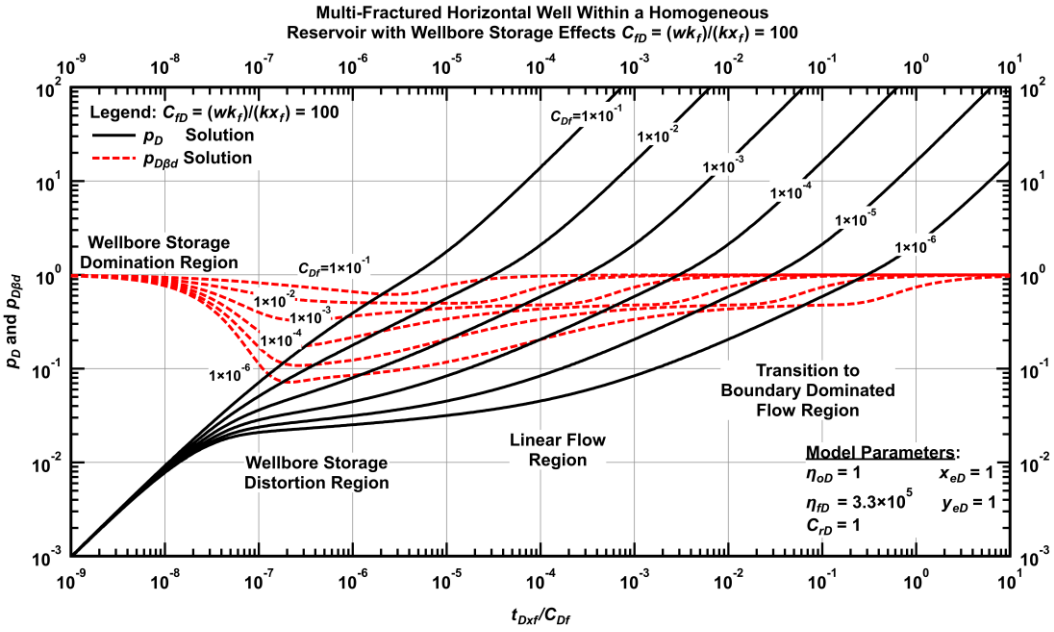

Figure A.4 — Log-log scale diagnostic plot for a multi-fracture horizontal well with varying wellbore storage effects within a homogeneous reservoir (C_{fD} = 100).

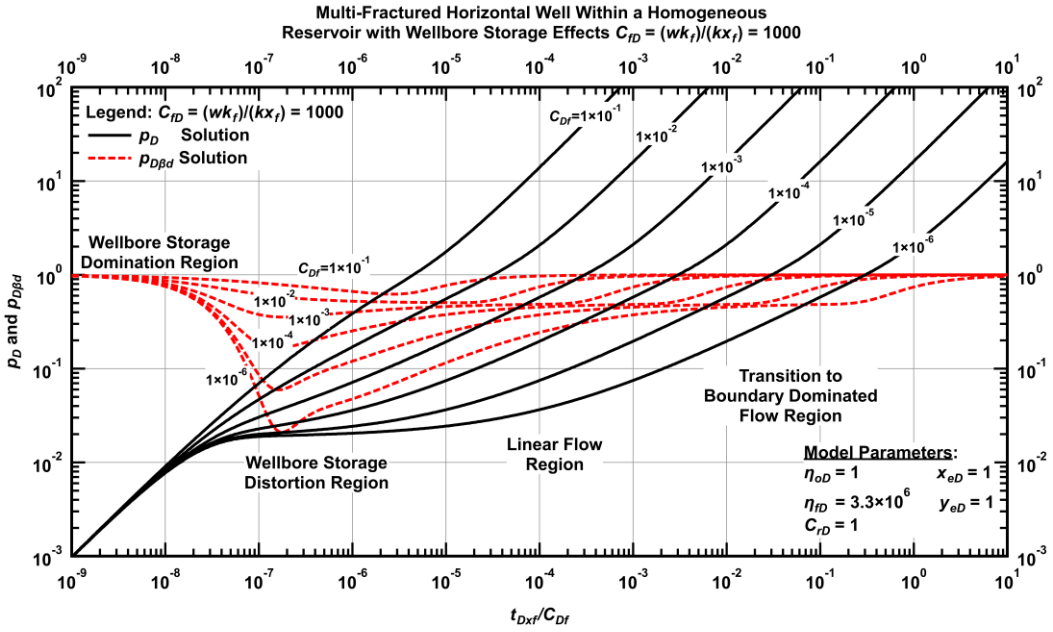

Figure A.5 — Log-log scale diagnostic plot for a multi-fracture horizontal well with varying wellbore storage effects within a homogeneous reservoir (C_{fD} = 1000).

A.2. Varying Hydraulic Fracture Conductivity For a Multi-Fracture Horizontal Well (MFHW) Within a Dual Porosity Reservoir with Pseudosteady-State Interporosity Flow Conditions.

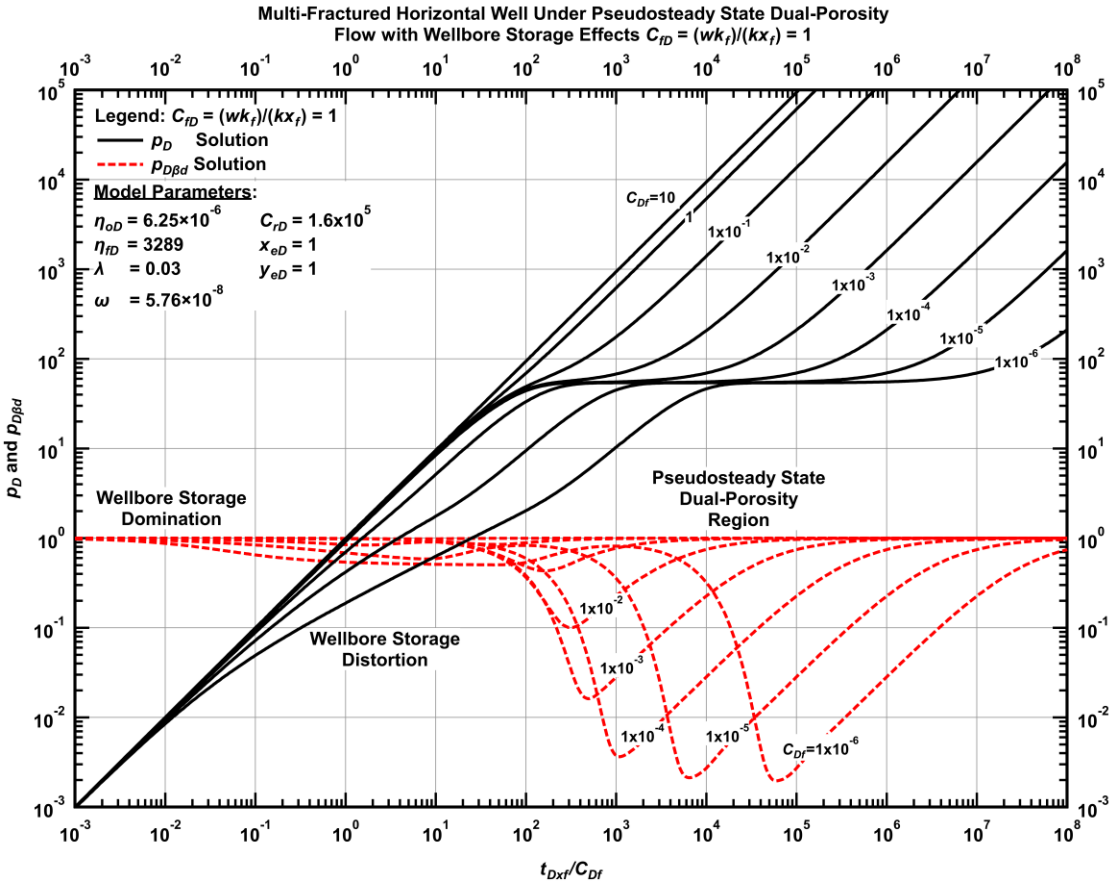

Figure A.6 — Log-log scale diagnostic plot for a multi-fracture horizontal well with varying wellbore storage effects, pseudosteady-state inter-porosity flow effects (C_{fD} = 1).

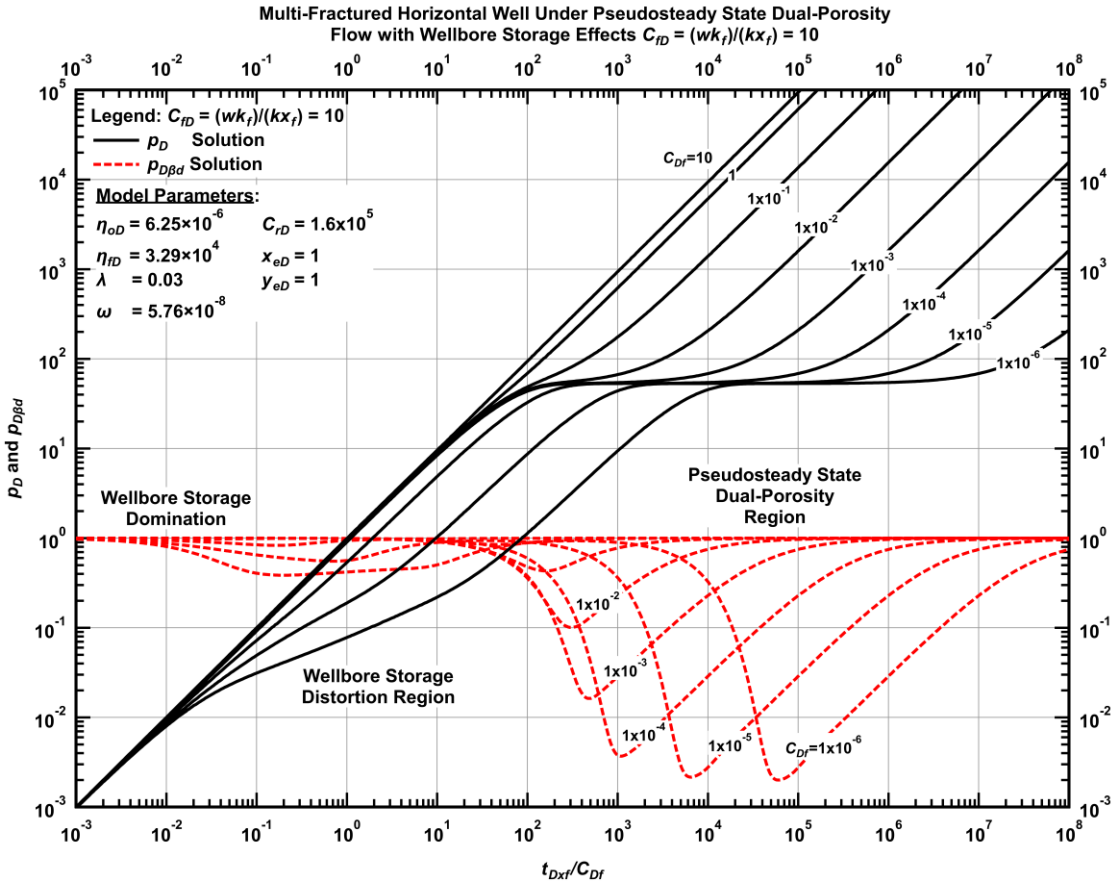

Figure A.7 — Log-log scale diagnostic plot for a multi-fracture horizontal well with varying wellbore storage effects, pseudosteady-state inter-porosity flow effects (C_{fD} = 10).

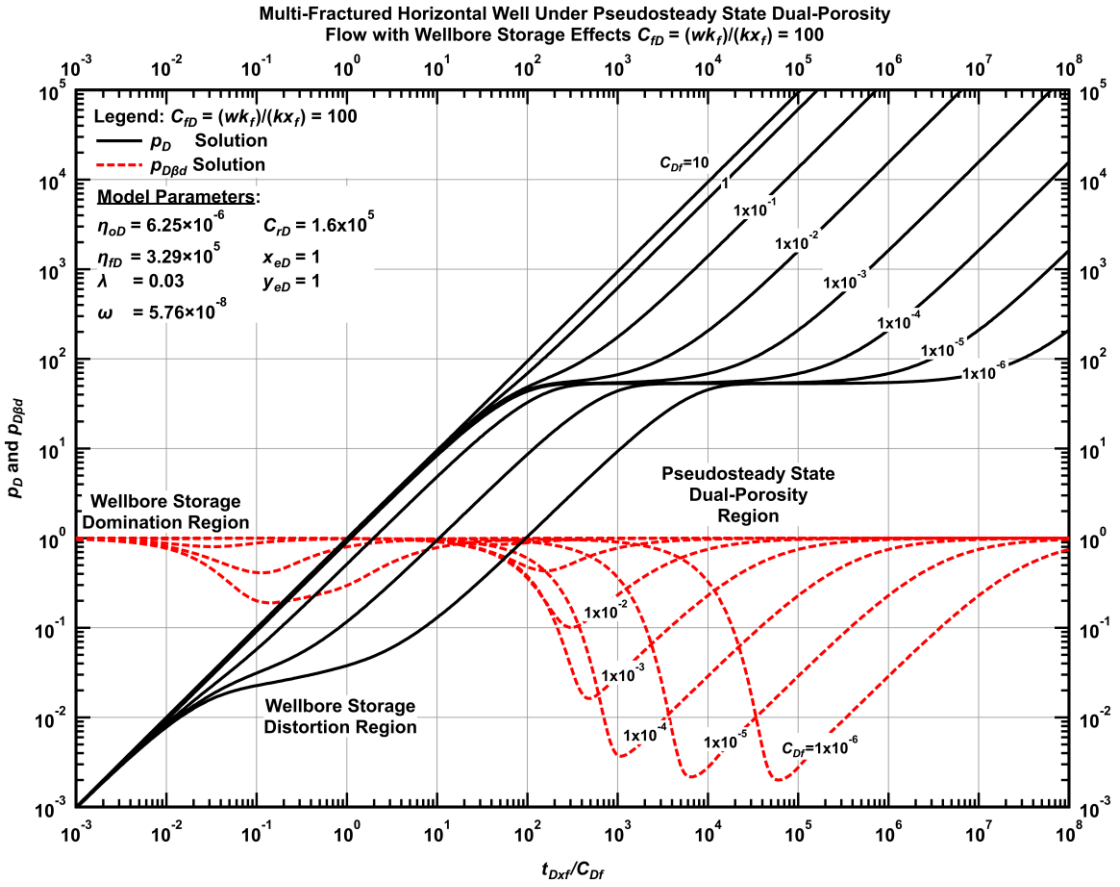

Figure A.8 — Log-log scale diagnostic plot for a multi-fracture horizontal well with varying wellbore storage effects, pseudosteady-state inter-porosity flow effects (C_{fD} = 100).

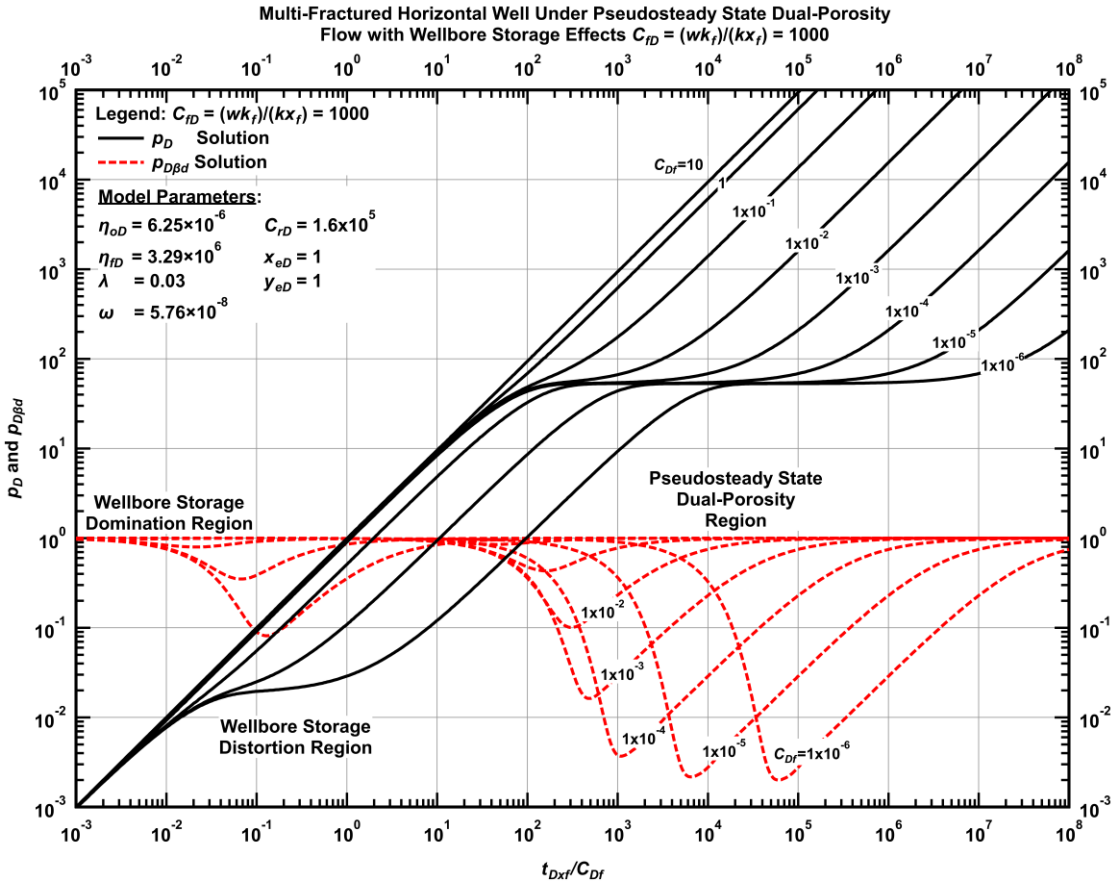

Figure A.9 — Log-log scale diagnostic plot for a multi-fracture horizontal well with varying wellbore storage effects, pseudosteady-state inter-porosity flow effects (C_{fD} = 1000).

A.3. Multi-Fracture Horizontal Well (MFHW) with Varying Flow-Capacity Ratio and Wellbore Storage Within a Dual Porosity Reservoir with Pseudosteady-State Interporosity Flow Conditions.

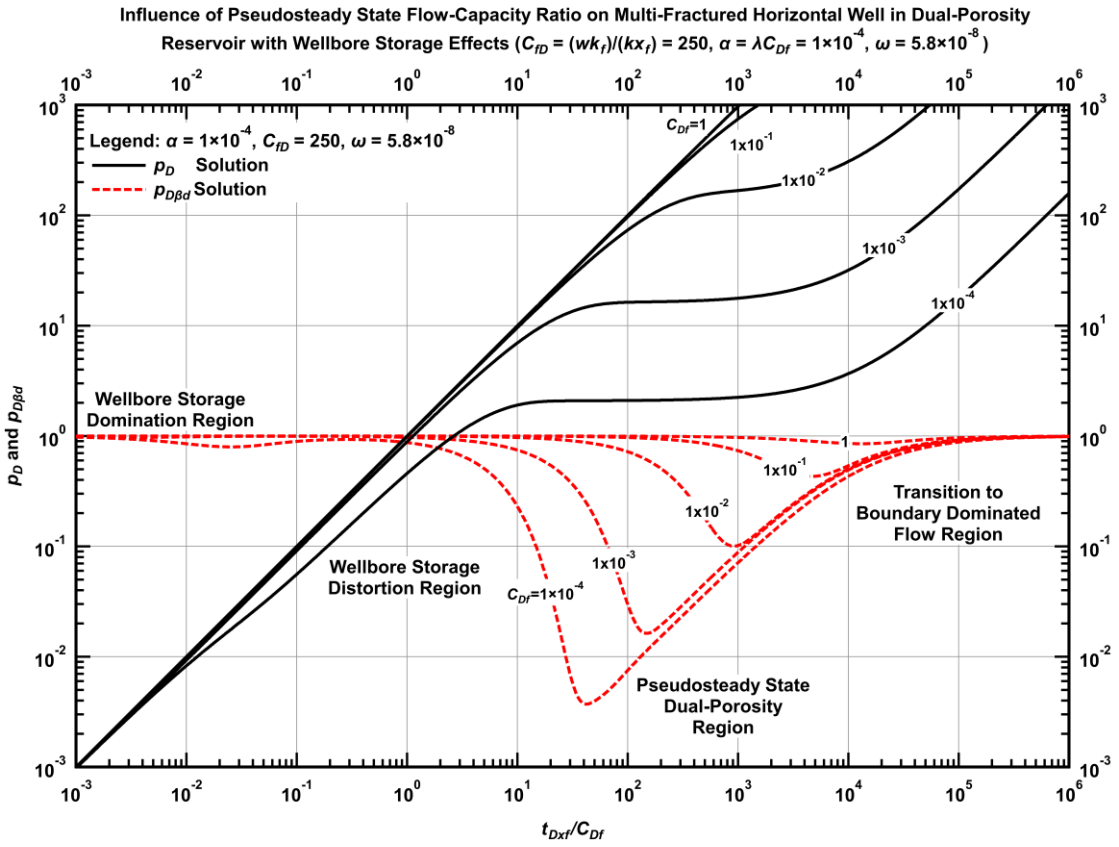

Figure A.10 — Log-log scale diagnostic plot for a multi-fracture horizontal well with varying wellbore storage effects and varying flow-capacity ratio, pseudosteady-state interporosity flow (C_{fD} = 250, α = 1x10^{-4}, ω = 5.8x10^{-8}).

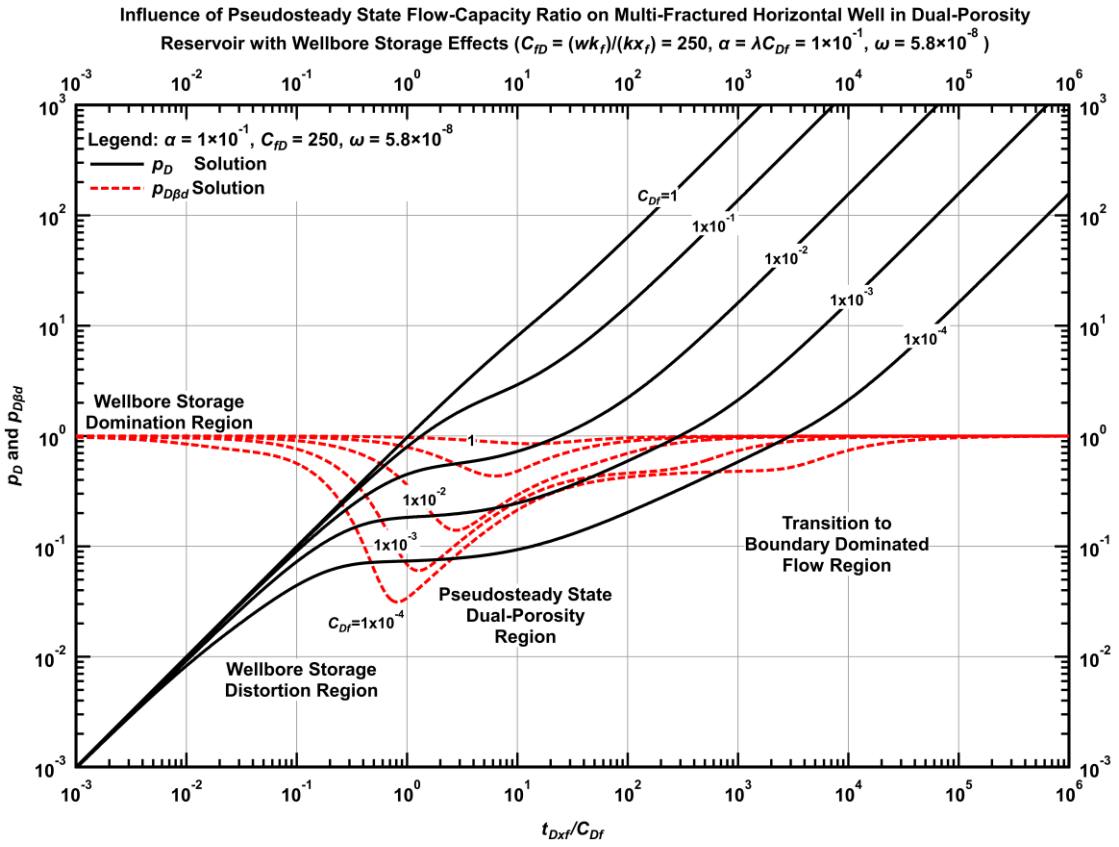

Figure A.11 — Log-log scale diagnostic plot for a multi-fracture horizontal well with varying wellbore storage effects and varying flow-capacity ratio, pseudosteady-state interporosity flow (C_{fD} = 250, α = 1x10^{-1}, ω = 5.8x10^{-8}).

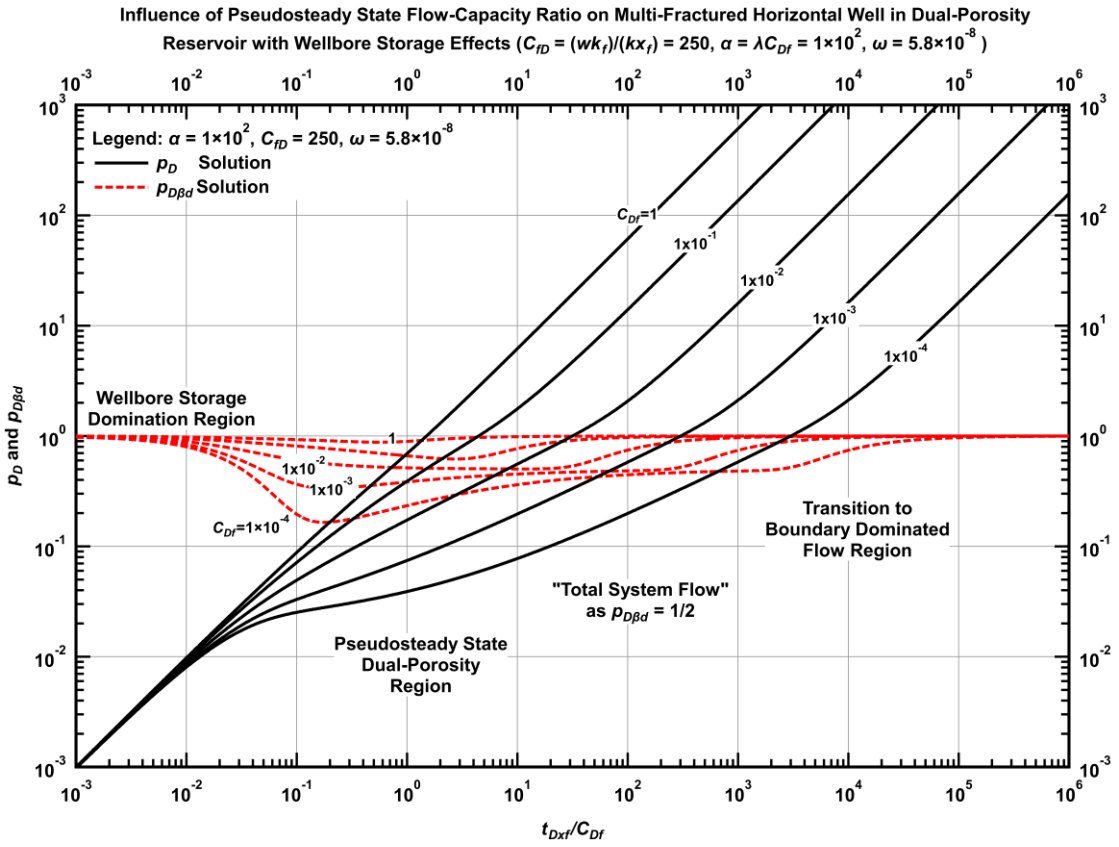

Figure A.12 — Log-log scale diagnostic plot for a multi-fracture horizontal well with varying wellbore storage effects and varying flow-capacity ratio, pseudosteady-state interporosity flow (C_{fD} = 250, α = 1x10^{2}, ω = 5.8x10^{-8}).

A.4. Multi-Fracture Horizontal Well (MFHW) with Varying Storativity Ratio, Varying Flow-Capacity Ratio, and Wellbore Storage Within a Dual Porosity Reservoir With Pseudosteady-State Interporosity Flow Conditions.

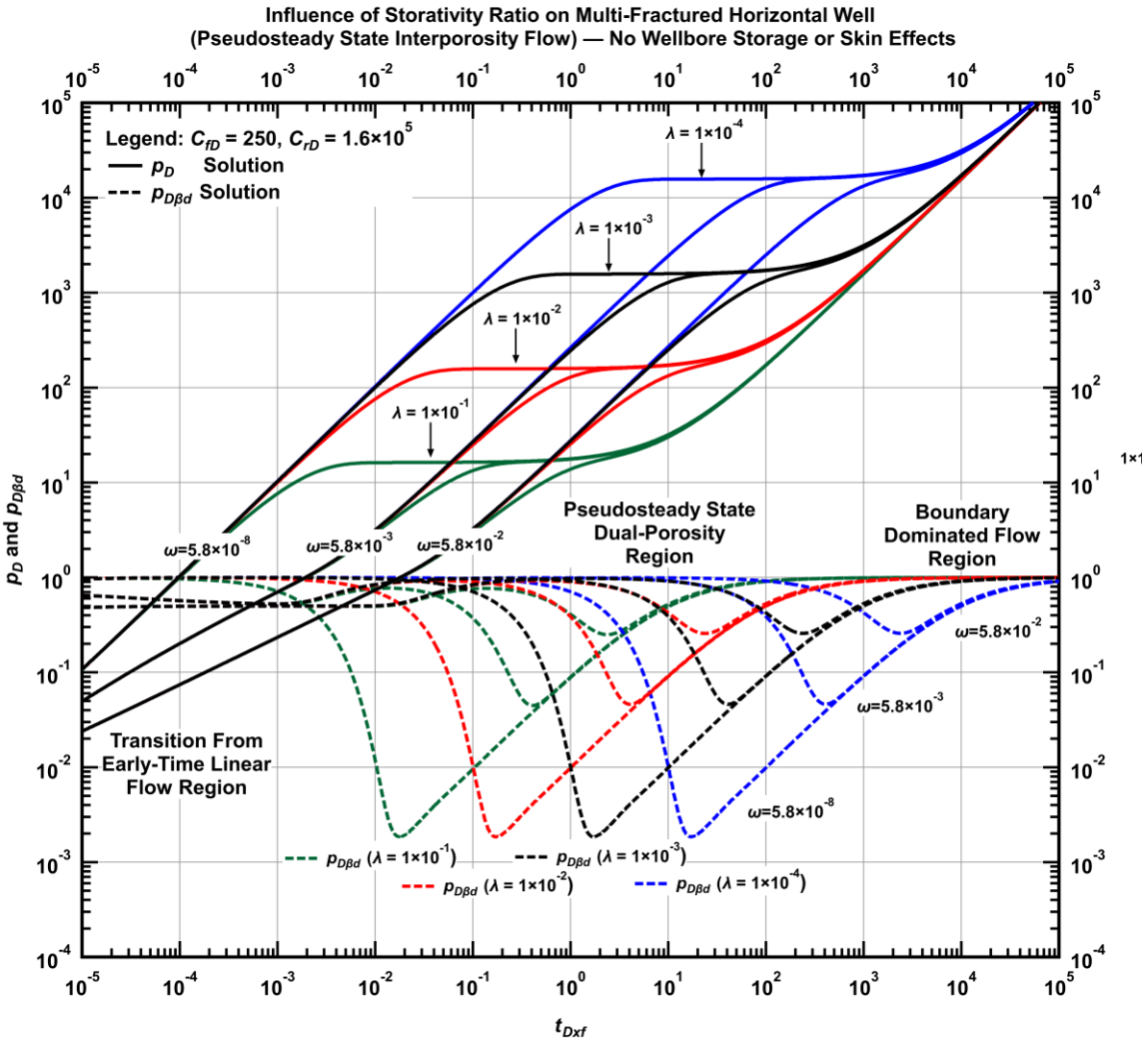

Figure A.13 — Log-log scale diagnostic plot for a multi-fracture horizontal well with varying wellbore storage effects and varying storativity ratio and flow-capacity ratio, pseudosteady-state interporosity flow.